1

A Detailed Study on Carbon Nanotubes: Properties, Synthesis, and Characterization

Nishant Tripathi[1], Prachi Sharma[1,2], Vladimir Pavelyev[1], Anastasiia Rymzhina[1], and Prabhash Mishra[1,3,4]

[1]Nanoengineering Department, Samara National Research University, 34, Moskovskoye Shosse, Samara, 443086, Russia
[2]Department of Electrical, Electronics and Communication Engineering, GITAM School of Technology, Bengaluru Campus, GITAM (Deemed to be University) NH 207, Nagadenehalli, Doddaballapura, Karnataka 561203, India
[3]Centre for Nanoscience and Nanotechnology, Jamia Millia Islamia, Jamia Nagar, New Delhi, 110025, India
[4]Center for Photonics & 2D Materials, Moscow Institute of Physics and Technology (MIPT), Dolgoprudny 141700, Russia

1.1 Introduction

The present chapter deals with the evolution of carbon allotropes, especially with carbon nanotubes (CNTs). CNTs are one of the most important nanomaterials of the carbon family. The invention of CNTs brought a real revolution in the field of nanoscience and nanotechnology. The astonishing properties of CNTs make them a suitable material for the development of applications in electronics, optoelectronics, medical, and in many other fields. Worldwide researchers are doing aggressive work on CNTs-based gas sensors, optical detectors, heat detectors, humidity sensors, transistors, nanoelectronics devices, and display applications [1, 2]. It has been observed that different types of applications based on CNTs require different types of CNTs. For example, sensors, especially for gas and optical applications, required horizontal aligned/network type of CNTs while field emission devices required vertically aligned CNTs. So, it has become very important to grow CNTs with selective structure and orientation [3]. Generally, CNTs can be grown by chemical vapor deposition (CVD), arc discharge, and laser ablation technique but among all the techniques CVD is the most preferable due to its capability to grow CNTs with selective properties. In general, the growth process of CNTs by using CVD system, a catalyst film deposited substrate is loaded into the chamber of CVD system, and then the chamber is heated around 800 °C in presence of a carrier gas; at 800 °C along with carrier gas, a hydrocarbon gas is supplied in CVD chamber for CNTs growth. CVD has lots of parameters to tune to decide CNTs' structural quality as well as morphology. The major parameters are the type of catalyst, catalyst

Chemically Modified Carbon Nanotubes for Commercial Applications, First Edition.
Edited by Jeenat Aslam, Chaudhery Mustansar Hussain, and Ruby Aslam.

deposition technique, catalyst engineering, growth temperature, growth duration as well as the type of carrier and hydrocarbon gas [3–5].

After synthesis of CNTs, its analysis became an important task. To analyze CNTs, researchers utilized various nanomaterial characterization tools such as scanning electron microscope (SEM), transmission electron microscope (TEM), atomic force microscope (AFM), Raman spectroscopy, and X-ray diffraction (XRD). SEM and AFM are useful for analyzing morphology of CNTs while TEM, Raman spectroscopy, and XRD are useful for the characterization of structural quality of CNTs.

All of the discussions mentioned motivated us to write a present book chapter. The chapter deals with evolution of Carbon from graphite, diamond, graphene to CNTs. It covers in detail various structures of CNTs, defects in CNTs, and their applications. It also covers the various synthesis and characterization techniques of CNTs. Finally, we made a broad discussion on the synthesis of selective CNTs.

1.2 Evolution of Carbon: Graphite to CNTs

The fundamental constituent or the building block of CNTs is Carbon. This group IV element of the periodic table is well known for its incredible ability to form crystalline solids and a variety of other compounds. It is placed in sixth position in the periodic table. Two out of its six electrons lie in 1s orbital, remaining electrons form sp^3, sp^2, or sp hybrid orbital. These four valence electrons constitute allotropes of Carbon such as CNT, diamond, graphite, graphene, and fullerenes [6]. It is an important fact that existing electronic bonds are very poor in the outer two orbitals as compared to the first orbital. Due to the weaker attraction of outer shell electrons than inner shell electrons, outer orbital electrons participate in electron hybridization. Small energy gradient between outer two orbitals (i.e. 2s and 2p) aids the overlapping of orbital wave functions favoring electron hybridization. There are three accessible mixing of atomic orbitals in carbon atoms making hybrid orbitals typically referred to as sp, sp^2, and sp^3 hybridization. In sp hybridization, one 2s and one 2p electrons participate in mixing (forming σ-bonds) and leaving two 2p electrons free of mixing (π-bonds). sp^2 hybridization involves the mixing of one's orbital electron and two 2p electrons. In sp^3 hybridization, all outer shell electrons of carbon atoms take part in mixing. The orbitals are focused on corners of a tetrahedron restricted to carbon atoms. According to hybridization, a carbon atom makes bonds with minimum one to maximum of four partners to produce compounds. Structural quality of carbon-based compounds and allotropes also depend on type of hybridization. For sp^l hybridization, $(l+1)$ σ bonds take charge to form generally one-dimensional local structure.

The linear chain compound of carbon i.e. "Carbyne" is an example of sp hybridization. sp^2 hybridization leads to the formation of two-dimensional structures such as graphene. 3D-structures such as diamond are formed by sp^3 hybridization. It is also noticed that in sp and sp^2 mixing one or two p orbital does not involve hybridization, instead showing their presence in the form π-bonds. Depending on orbital mixing carbon has many allotropes and among these

amorphous carbon, diamond, graphite, graphene, and CNTs have received a great amount of attention [7]. These allotropes of carbon exhibit a part or completely different properties in nature. For their commendable and extraordinary multidimensional properties be it CNTs, graphene or diamond, and others, allotropes of carbon have become a hot cake for research investigations.

1.2.1 Graphite

The word graphite is taken from a Greek word "graphein" i.e. "write." Pencil, which is an attractive and widely used tool for writing and drawing, is made from it. It was invented by Debye et al. in 1917 [8]. Graphite is a combined structure of layers. Each layer is called Graphene [9]. In graphite structure, carbon atoms are situated in hexagonal fashion on the *XY* plane [10]. The distance between carbon atoms in a single layer of graphite is 0.142 nm. The separation distance between layers of graphite is approximately 0.335 nm [11].

The graphene layers are held together by weak van der Waals forces to form solid structure graphite. Each carbon atom is situated on edge of hexagon having three σ-bond in sp^2 hybridization form in which three valence electrons participate in hybridization and one valence electron exists in p_z orbital creating two-dimensional electron gas in the form of π-bond or cloud. It is spread all over on individual *XY* planes of graphite. Due to the mobility of said electron gas, graphite shows electrical conductivity. It is more reactive than diamond. The separation distance between the nearest two carbon atoms on an individual layer of graphite is around 0.142 nm that is approximately equal to band order of 1.5 and two times larger than the aromatic carbon atom's covalent radius. The separation gap among the nearest two layers of graphite is approximately two times of van der Waals radius. The weak van der Waals interaction within layers of graphite causes the layers of graphite to easily move along the *XY* plane. Generally, two types of graphite are found in nature abundantly: a stable form that is hexagonal or α-graphite and rhombohedral or β-graphite. β-graphite is more abundant in nature than α-graphite. By heat treatment, β-graphite can be changed into α-graphite. Other than these two, a few more types of graphite are found in nature. Sometimes, due to some disorder in stacking, no more attraction exists between layers and hence individual layers of graphene or graphite randomly turn around the *z*-axis and move in the *XY* plane resulting in a turbostratic structure.

1.2.2 Diamond

Diamond is an allotrope of carbon with sp^3 hybridization. Every carbon atom in diamond is bonded to four nearest carbon atoms. Each diamond cell has a tetrahedron structure with a bond length of 154.45 pm. Mainly, two types of structures of diamond are found: cubic and hexagonal. Cubic structure is more available than hexagonal [12, 13]. Hexagonal-shaped diamonds are very precious and rare to find. It was first found in 1967 in a meteorite. Still, there is a possible way to synthesize artificially hexagonal type diamond from graphite by heat treatment of graphite

under high pressure with ambient temperature along the vertical axis. Some other structures are also found in which nitrogen molecules are mixed with carbon atoms. Some noticed nitrogen-contained diamonds are Ia, Ib, IIa, and IIb. If nitrogen contamination is like platelets then it is Ia structure of C_3N composition. In Ib type nitrogen, molecules are homogeneously spread all over the structure. And, if the diamond structure has null nitrogen then it is called IIa. The last structure has a very small probability of being in nature. The last type, i.e. IIb, is a semiconducting diamond. In that case, nitrogen is completely absent. Instead of nitrogen, IIb type of the diamond structure has some contamination of aluminum. In a normal diamond unit cell, eight atoms exist having face-centered cubic packing. The lattice constant of diamond lattice is 356.68 pm [14–18]. Another noticeable point about diamond's structure is that it's packed in a sphalerite kind instead of dense packing. Its structure is a penetration of two faces. Its centered cubic lattice can be moved along unit cell space diagonal. Another thing is that if diamond is heated with specific conditions, i.e. 3750 °C temperature and 1840 psi pressure, it is converted to graphite. It is also possible to make a hexagonal structure like its cubic type structure from tetrahedrons of carbon with different configurations. In the specified configuration, the cell is made from four carbon atoms with lattice parameters $a_0 = 252$ pm and $c = 412$ pm [15].

1.2.3 Graphene

As described in Section 1.2.1, if a single layer of graphite is peeled-off from the bulk material, then it is called graphene. It is a single planar structure containing covalent bonded carbon atoms [19] thus also known as planar allotrope of carbon. Buckyballs, nanotubes, and graphite are allotropes of graphene. If graphene is folded in a shape of sphere then it becomes the buckyball or if rolled along any of its axes then it takes the form of a nanotube. Stacked layers of graphene through its *XY* plane are graphite. Therefore, graphene may be called a generator of three allotropes of carbon. Thus it is vital to study the properties of graphene to understand the properties of CNTs and the other two allotropes. The 2s, $2p_x$, and $2p_y$ electrons interact in hybridized fashion giving graphene its characteristics such as physical and electrical ones [19].

sp^2 hybridization results in the formation of very stable covalent bonds (σ-bonds) on graphene surface which is the reason for graphene and CNTs being the strongest material with superior mechanical properties among other materials known. Not hybridized atomic $2p_z$ orbital forms π-bonds normal to *XY* plane due to the electron gas delocalization. These π-bonds provide graphene with distinctive electronic properties [20]. Structurally, graphene has two types of lattice arrangements: direct and reciprocal lattice.

1.2.3.1 Direct Lattice

The honeycomb structure of direct lattice graphene can be explained by ball and stick model. In the ball and stick model, carbon atoms are denoted by ball and sticks represent σ-bonds. σ-bonds of graphene have a bond length around 1.42 Å. Such type of lattice may be considered as a Bravais lattice. The Bravais lattice basis is 2

given as two π electrons per unit cell and depicts enhanced electronic properties of graphene [21]. The primitive unit cell of mentioned honeycomb lattice may be taken as an equilateral parallelogram. The parallelogram side length is as following:

$$a = \sqrt{3}\,(\text{length of a } \sigma\text{-bond}) = 2.46\ \text{Å} \tag{1.1}$$

The vectors of primitive unit cell are as following:

$$a_1 = \left(\frac{\sqrt{3}a}{2}, \frac{a}{2}\right) \tag{1.2}$$

$$a_2 = \left(\frac{\sqrt{3}a}{2}, \frac{a}{-2}\right) \tag{1.3}$$

where the vector $|a_1| = |a_2| = a$ describes the separation distance between two nearest carbon atoms.

$$R_1 = \left(\frac{a}{\sqrt{3}}, 0\right) \tag{1.4}$$

$$R_2 = (-a_2 + R_1) \tag{1.5}$$

$$R_2 = \left(-\frac{a}{2\sqrt{3}}, -\frac{a}{2}\right) \tag{1.6}$$

$$R_3 = (-a_1 + R_1) \tag{1.7}$$

with $|R_1| = |R_2| = |R_3| =$ length of σ-bond.

1.2.3.2 The Reciprocal Lattice

The rotated lattice with an angle of 90° with reference to the direct lattice is called a reciprocal lattice of graphene [17]. Similar to the direct lattice, the reciprocal lattice also has carbon atoms arranged in a honeycomb structure. The vectors of said lattice are given below:

$$b_1 = \left(\frac{2\pi}{\sqrt{3a}}, \frac{2\pi}{a}\right) \tag{1.8}$$

$$b_2 = \left(\frac{2\pi}{\sqrt{3a}}, -\frac{2\pi}{a}\right) \tag{1.9}$$

where $|b_1| = |b_2| = \dfrac{4\pi}{\sqrt{3a}}$.

1.2.4 Carbon Nanotubes

The history of Carbon tubular structures start after the invention of electron microscopes in 1950 [22]. In 1952, a hollow tube of carbon was invented by a Russian researcher, Radushkevich and Lukyanovich, however, the article did not gather much attention being published in a local language [23]. Baker et al. again investigated related structure in 1972 [24]. In 1976, Oberlain et al. described single

cylinder hubs in a graphite structure of carbon fibers [25]. Finally, in 1991 Sumio Iijima, an electron microscopist, discovered the cylindrical structure of carbon while analyzing fullerenes, another allotrope of carbon [26]. His discovery caught the attention of worldwide researchers in the field of nanotechnology. Almost two years later, the same group of researchers achieved another milestone in the field of nanotechnology with the invention of single wall carbon nanotubes (SWNTs). CNT is one of the essential allotropes of graphene and is formed when a graphene sheet is rolled into a seamless hollow tube. Practically, it is impossible to roll a graphene sheet into a cylindrical structure because of its ultra-small dimensions. It is only said to understand the structure of CNTs. Generally, diameter of CNTs lies between 0.5 and 5 nm thus termed as nanotubes. The length of CNTs, however, falls from a few mm to several cm [7]. CNTs are also called tubical fullerenes. Generally, CNTs are found in two structures: (i) SWNTs (see Figure 1.1a) and (ii) multi wall carbon nanotubes (MWCNTs) (see Figure 1.1b). If single graphene sheet is rolled to make CNTs then it is called SWNTs and if more than one graphene sheet is concentrically rolled in the "Russian dolls model" then the tubes are called MWNTs. SWNTs are discussed below followed by an introduction about the MWNTs.

1.2.4.1 SWNTs: Types and Structure

Based on structure, SWNTs are divided in three categories:

i. Zigzag
ii. Armchair
iii. Chiral

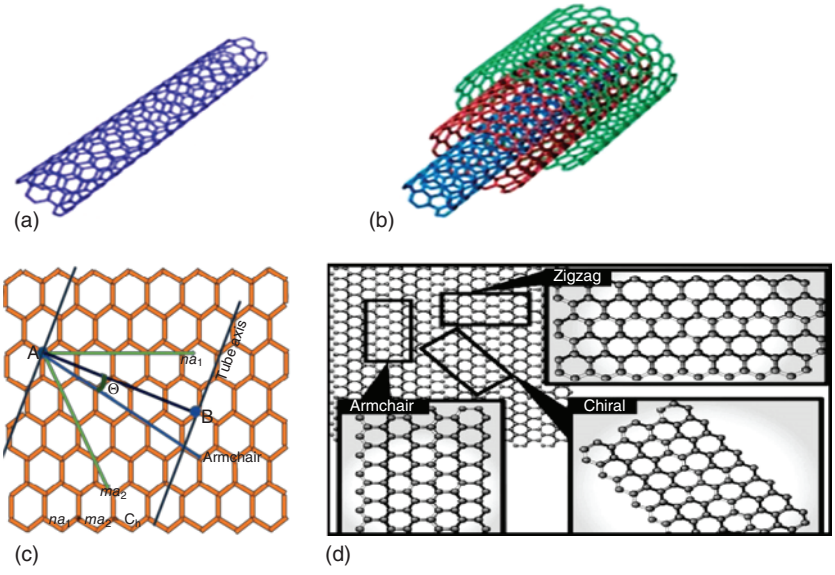

Figure 1.1 Figure (a) and (b) show the schematic diagram for SWNTs and MWNTs, respectively. Figure (c) shows the honeycomb structure of carbon atoms; (d) shows different types of CNTs structure. Source: Ahmad Aqel et al. [27]/with permission of Elsevier.

The types of SWNTs depend on the type of rolling of graphene sheets, which are the basis of the CNTs tubular structure. It is possible to calculate the chirality (helicity) as well as the diameter of SWNTs from a vector, called the chiral vector C_h. It is defined as

$$C_h = na_1 + ma_2$$

where $n, m = 1, 2, 3, \ldots$ with notation as (n, m).

The diameter of SWNTs according to the said model is calculated by the following equation:

$$d = \frac{\text{Chiral Vector}}{\pi} \tag{1.10}$$

$$d = \frac{\sqrt{3} * b\sqrt{n * n + nm + m * m}}{\pi} \tag{1.11}$$

where b has the value of 0.142 nm, which represents the carbon–carbon bond length. It is observed that the diameter of CNTs strongly depends on its chirality. A CNT having (5,5) chirality tends to have a smaller diameter than a CNT with (10,10) chirality. The steps for calculating chirality are as mentioned below [27, 28]:

I. Plot the tube axes. The tube axes are the nanotubes edges. If the tube axes join with each other in the form of a cylinder then it becomes nanotubes (see Figure 1.1c).
II. Mark a point A along the tube axis where the tube axis interacts with carbon atoms.
III. Draw the armchair line (thin green line) by finding any point along the tube axis that travels across each hexagon, separating them into two equal halves.
IV. Take point B on the second tube axis at the intersection of the tube axis and carbon atoms. It should be the nearest intersection point from the armchair line.
V. Draw a line AB representing the chiral vector C_h. The chiral vector is equivalent to the CNTs circumference.
VI. Angle θ between the armchair line and chiral vector decides the types of SWNTs.
VII. If the armchair line and chiral vector overlap each other, i.e. when $\theta = 0°$ $(n = m)$, then the resulting SWNTs are called the armchair SWNTs (see Figure 1.1d).
VIII. If the said wrapping angle is $\theta = 30°$ $(m = 0)$, then zigzag nanotubes are formed (see Figure 1.1d).
IX. If the wrapping angle θ is between 0° and 30°, then the fabricated SWNTs are called chiral.

Among all types of CNTs, chiral type CNTs have the superior place. Because chirality is an elemental theory to investigate different configured CNTs and their relative electronic band structures. Therefore, it is important to understand the concept and its application to identify CNTs structure. Table 1.1 shows parameters and their relative equations for CNTs.

Table 1.1 Various parameters for SWNTs.

S. no.	Symbol	Name	Chiral CNT	Armchair CNTs	Zigzag CNTs
1.	C_h	Chiral vector	$C_h = na_1 + ma_2 = (n,m)$	$C_h = (n,m)$	$C_h = (n,0)$
2.	C_h	Length of chiral vector	$C_h = \lvert C_h \rvert = a\sqrt{n^2 + nm + m^2}$	$C_h = a\sqrt{3n}$	$C_h = an$
3.	d_t	Diameter	$d_t = \frac{a}{\pi}\sqrt{n^2 + nm + m^2}$	$d_t = \frac{an}{\pi}\sqrt{3}$	$d_t = \frac{an}{\pi}$
4.	Θ	Chiral angle	$\cos\theta = \frac{2n + m}{2\sqrt{n^2 + nm + m^2}}$	$\theta = 30°$	$\theta = 0°$
5.	N	Number of hexagons/cells	$N = \frac{2C_h^2}{a^2 g_d}$	$N = 2n$	$N = 2n$

1.2.4.2 Chirality

The word chirality comes from the Greek language that means HAND. It is used to represent reflection symmetry between an object and its mirror image. In general, a chiral object is anti-symmetric to its mirror image. For example, if we take the mirror image of our left hand and try to superimpose it on our left hand, it does not accurately superimpose, indicating that hands are chiral objects. Similarly, CNTs that are superimposed to their mirror image are called achiral CNTs. Zigzag and armchair CNTs are examples of achiral CNTs.

1.2.4.3 Electronic Properties of CNTs

Electronic properties of CNTs provide great opportunities in nano-electronic research applications. Ultra-small dimensions and ultra-symmetric structures create remarkable quantum effects and electronic properties of nanotubes. Due to the circumferential confinement effect on tubes, SWNTs and MWNTs [28–33] show the quality of a quantum wire. Experimental investigations have proved that MWNTs and the rope of SWNTs behaved like a parallel assembly of single SWNTs. The electronic conductance for said assembly is given by

$$G = G_o M = \left(\frac{2e^2}{h}\right) M \tag{1.12}$$

where, the calculated value of the quantized conductance G_o is 12.9 $k\Omega^{-1}$. Another parameter used in the equation, i.e. M is the measurement of exact conducting channels, and its exact value for an ideal defect-free SWNT is 2. The value of M is determined by the intrinsic properties of nanotubes, coupling between tubes impurities, defects in the structure of tubes, interaction with the substrate, and on contacts made for electronic connections. Therefore, the experimental value of conductance is less than the quantized value [34].

Many research groups reported about graphite's resistivity. It depends strongly on the quantity of graphite taken for analysis. The best quality graphite has the resistivity around 0.4 μΩm at room temperature [35]. In the case of CNTs, the MWNTs,

as well as the rope of SWNTs, have much higher resistivity than the best quality graphite. It is also reported that the resistivity of the nanotubes mentioned above decreases with temperature. These results were found due to a random orientation of nanotubes on the substrate. The same measurements were made for purified CNTs aligned between four electrodes and were found to be much less than 0.4 μΩm [34, 36]. In defect-free nanotubes, π electrons are more distributed as compared to graphite. It happens due to σ–π re-hybridization. These conditions made graphene more conductive as compared to graphite [34]. Therefore, CNTs are called 1-D conductors.

1.2.4.4 Optical Properties of CNTs

Defect-free SWNTs have a direct band gap. They also have a well-defined structure of the sub band. Such type of structure is considered ideal for optical applications. Optical spectra of SWNTs may be obtained by resonant Raman spectroscopy [35] and by fluorescence spectroscopy [36, 37]. An optical spectrum obtained for grouped SWNTs, as well as for graphite under compression, is shown in Figure 1.2. Three important peaks that are found in SWNTs are invisible in graphite and attributed to symmetric transitions between the lowest sub-bands in semiconducting (A and B) and metallic (C) tubes. Generally, it is found that grown CNTs area a mixture of semiconducting and metallic tubes. In CNTs, the measured peak position and intensity of optical spectra provide information about the electronic structure or tube chirality or (D, Θ). Thus, for a detailed composition investigation of CNTs, optical spectra become indispensable. To understand the optical properties of CNTs, it is necessary to understand their band structure and density of states (DOS), which is already discussed in the electronic dispersion Section 1.2.4.3.

The optical transportation is only possible when electrons or holes are triggered from a lower energy level to a higher energy level. The energy required for optical

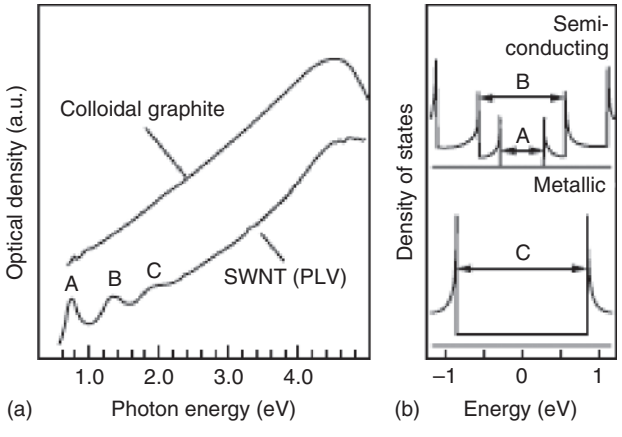

Figure 1.2 Figure shows the UV–vis–NIR analysis for various SWNTs samples. Figure (a) shows the absorbance spectra of SWNTs as well as of colloidal graphite. Figure (b) shows plots of the density of states for semiconducting and metallic CNTs. Source: Hagen and Hertel [37]/with permission of American Chemical Society.

transactions is donated by E_{pq}. There are two selection rules that are defined for that. First, if $p - q = 0$, it is defined for inter-band transitions. It is symmetric to the Fermi energy of the polarized light along the tube axis. Second, it requires light that is normal to the tube axis. However, it does not appear in optical spectra. It happens due to very weak transitions [37].

1.2.4.5 Chemical Properties of CNTs

Due to ultra-small dimensions and ultra-large specific area with σ–π re-hybridization, CNTs are highly sensitive to chemicals and environmental interactions. It is important to study the chemical properties of CNTs such as opening, wetting, filling, adsorption, charge transfer, doping, and intercalation for application purposes.

Opening It is reported by several research groups that the ends of CNTs are more reactive than their complete structure. CNTs' ends have metallic catalyst particles with a large curvature on their open end. Therefore, many approaches have been focused on opening CNTs ends such as treatment with acids, plasma treatment, etc. [38, 39].

Wetting and Filling CNTs are hydrophobic in nature. Mostly aqueous solvents are unable to wet CNTs. However, some organic elements, HNO_3, S, Cs, Rb, and Se as well as some oxides Bi_2O_2 are able to wet CNTs, if they are pressurized with capillary pressure. Using this technique, some other nonwetting elements may also be injected into CNTs. The capillary pressure for nanotubes is proportional to $\left(\frac{1}{D}\right)$ [40].

Adsorption and Charge Transfer It is expected that CNTs have enhanced molecular adsorption as well as charge transfer. Researchers have reported that CNTs show very good adsorption and charge transfer from oxygen to CNTs at room temperature. The localized sites on CNTs where pores exist, interstitials in tube bundles, the surface of CNTs as well as a groove between two attached CNTs are the perfect places for charge transfer and adsorption. In fact, the mentioned sites show the capability of CNTs for adsorption and charge transfer.

The CNTs property discussed above is successfully used in NO_2, $C_6H_5NO_2$, C_6H_6, NH_3 as well as in CH_4 sensing. When these molecules interact with CNTs, a change in CNTs resistance is observed. It is possible to design electronic device for sensing application on that principle [41, 42].

Chemical Doping, Intercalation, and Modification The discussed adsorption method may be used for noncovalent bonding doping of CNTs to make p-type as well as n-type CNTs to enhance their electronic conductivity. Intercalation of alkali metals is also used to enhance electronic conductivity. Researchers reported on behalf of the experimental evidence that alkali metals diffuse into inter tube space or defects that exist in CNTs, and hence enhance the CNTs charge transfer ability. To enhance the electrochemical capacity of CNTs, CNTs itself can be used as electrodes. In CNT-based electronic devices for energy production or harvesting, the flow of electrons is generated by reduction and oxidation reactions occurring at the electrodes [43–47].

1.2.4.6 Defects in CNTs

Defects, being a deterministic factor for the physical and chemical properties of a nanomaterial, are considered significant. Although nanomaterials like CNTs are perfect and have unique electrical and mechanical properties which change due to presence of certain defects such as vacancies, heptagon–pentagon pairs type transformations, doping, and interstitials, edges and adatoms (see Figure 1.3) [49], resulting CNTs can be used for further applications, such as sensing, hydrogen storage, and drug delivery systems.

Structural Defects Structural defects in CNTs arise due to their topology distortion caused by the introduction of pentagonal, heptagonal, and octagonal rings into the hexagonal carbon network, affecting nanotubes electrical properties resulting in a conical structure with sharp tips due to the presence of a pentagonal ring at the nanotubes peaks (as shown in Figure 1.3a,b). Also, different vertex angles are obtained by a pentagon insertion into a hexagonal carbon graphitic structure leading to 30° bend dictating that pentagon and hexagon are separated maximally that is they are placed opposite to each other (as shown in Figure 1.3c) and 0° bend is obtained when both structures are combined. Thereby, we can conclude that the vertex angles can indicate the count of hexagon–pentagon pairs present in the CNTs.

A spiral CNT (as shown in Figure 1.3d) is an out-of-plane structure obtained by introducing pentagonal and heptagonal rings in a perfect graphitic sheet and then rolling it with a rotation angle. Atoroidal CNT (as shown Figure 1.3e) is an in-plane structure obtained by connecting CNTs of various diameters by inserting pentagons and hexagons [50].

Bond Rotation Thrower stone wales (TSW) type defects produced by bond rotation in the nanotube are due to 90° rotation of C—C bond in a hexagonal network such as in fullerenes, resulting in a translation of two heptagons and pentagons (as shown in Figure 1.3f) [48–51]. Unlike the conical-end structure formed in structural defects, this TSW type defect does not result in large curvature deviations of the nanotube. TSW type defects cause a plasticity failure at elevated temperatures and can alter the chirality of CNTs. Further elongation of the tube at the defect location can lead to the nanotube collapse. Its significance lies in the innovation of nanoelectronic devices [52].

Doping-Induced Defects In order to increase the conductivity of a CNT, dopant atoms can be inserted (see Figure 1.3g) in the carbon lattice. Another method consists of the functionalization of nanotubes, which makes it suitable for biochemical and gas sensing purposes. The boron (p-type dopant) and nitrogen (n-type dopant) atoms in the internal CNT structure are used to sense carbon monoxide and water molecules. The boron (B) atom doping is carried out by arc discharge method using BN-rich as an anode and the nitrogen (N) atom doping is carried out by ferrocene-melamine mixture pyrolysis at high temperatures [53]. As a result of doping, both nanotubes become metallic in nature with no band-gap in comparison with the undoped lattice structure. Other atoms used for doping purposes are P, S, and Si in addition to

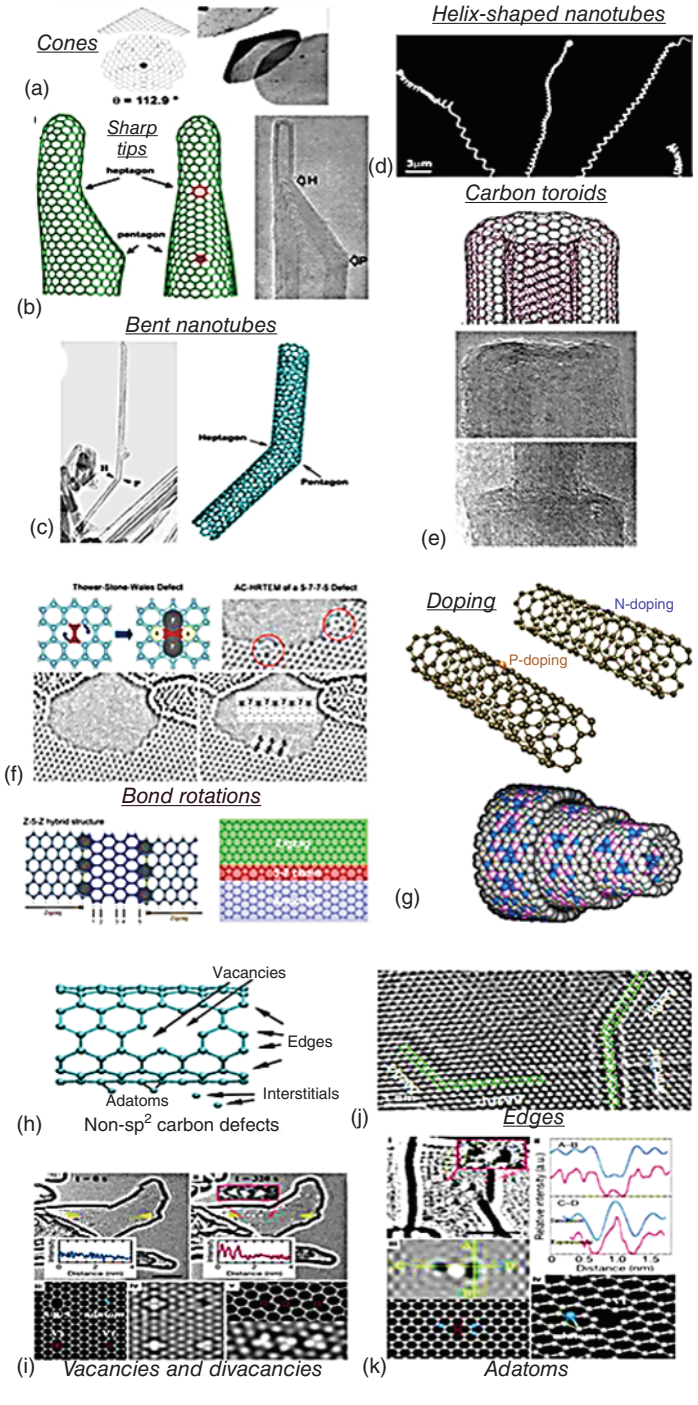
Cones
(a)
θ = 112.9 °
Sharp tips
heptagon
pentagon
(b)
Bent nanotubes
Heptagon
Pentagon
(c)
Helix-shaped nanotubes
(d)
Carbon toroids
(e)
Thrower-Stone-Wales Defect
AC-HRTEM of a 5-7-7-5 Defect
(f)
Bond rotations
Doping
N-doping
P-doping
(g)
Vacancies
Edges
Interstitials
Adatoms
(h)
Non-sp2 carbon defects
(j)
Edges
(i)
Vacancies and divacancies
(k)
Adatoms

Figure 1.3 Figure shows the various defects involved in CNTs. Figure (a) shows the graphitic conical shape fabricated on the CNT tip. Figure (b) shows the presence of pentagon and heptagon impurities on the CNT tip. Figure (b) and (c) show bending and helices types of CNTs. Figure (e) represents the joining of two concentric CNTs by a hemitoroidal cap. Figure (f) shows the TEM analysis as well as molecular model of the TSW defect for the conversion of four hexagons into two pentagons and two heptagons. Figure (g) demonstrates nitrogen and phosphorous doped CNTs. Figure (h) shows simulated images of various non-sp^2 defects that occur in CNTs while figure (i–k) show experimentally produced vacancies, edges, and adatoms defects, respectively. Source: Lehman et al. [48]/with permission of Elsevier.

B and N atoms; all of them alter the reactivity of the nanotube, enhancing the binding energy of the sensing molecule with the doped species [54–57].

Non-sp^2 Carbon Defects These non-sp^2 hybridized defects in the CNT structure are formed due to dangling bonds, other than carbon atoms found in the lattice structure, or can be caused by vacancies, adatoms, and opened or closed nanotubes as shown in Figure 1.3h. Adatoms remain as dopants on the surface of nanotubes, in which the lattice structure stays undisturbed. Depending on the ratio between the lower and upper levels of occupied molecular orbitals of adatoms and the Fermi level of the tube, the electrons of dopant atoms are transmitted or absorbed.

1.2.4.7 CNTs Properties Modification by Chemical Functionalization Process

CNTs functionalization helps to improve their processibility and solubility as well as to mix the unique features of materials attached to CNTs with their own properties [58–63]. Chemical bounds can tailor the CNT interaction with other systems like biopolymer matrices, solvents, polymers, and other nanotubes. Approaches to CNTs functionalization are divided into noncovalent (physical) and covalent (chemical) as interactions between CNTs and attached elements as can be seen in Figure 1.4a–e [64, 66]. A distinction that is more detailed can be made if we divide the functionalization of MWNTs and SWNTs, as well as that of tube bundles and individual tubes [67].

Covalent functionalization constructs from the functional entities covalent linkage on the surface of CNT. It can be further divided into indirect covalent functionalization with carboxylic groups and direct covalent side wall functionalization. Direct covalent side wall functionalization appears due to hybridization change from sp^2 to sp^3 along with a conjugation loss. Indirect covalent functionalization (also known as defect functionalization) utilizes defect sites that already occur in the CNT. These sites can appear in a form of open ends as well as in the form of holes in the walls with attached, for example, carboxylic groups. Oxygenated sites also can be considered as defects [65]. Acid chloride, in major cases converted from carboxylic acid groups, is utilized to increase the CNTs reactivity with further treatment via amidation or esterification reaction [68].

Noncovalent functionalization is founded primarily on secondary interactions like van der Waals' forces or π-stacking. All the mentioned above functionalization methods are exohedral derivatizations. Endohedral CNTs functionalization (the

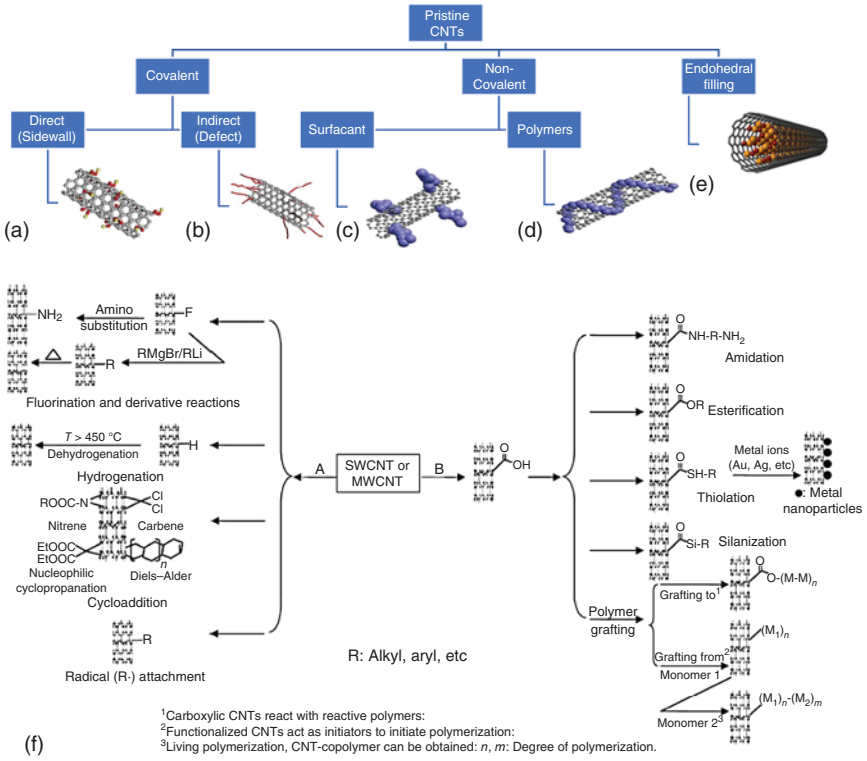

Figure 1.4 Functionalization types of CNTs: (a) chemical side wall functionalization, (b) defect-group functionalization, (c) physical exohedral functionalization with surfactants, (d) physical exohedral functionalization with polymers, (e) endohedral functionalization. For A–C approaches, the nanotubes are idealized, however, defects can be observed in reality. Source: Muhammad-Ahson Aslam et al. [64]/MDPI/Public Domain CC BY. Figure (f) CNTs covalent functionalization strategies: A-route represents side wall functionalization, B-route demonstrates defect functionalization. Source: Ma et al. [65]/ with permission of Elsevier.

tubes filling with atoms or small molecules) is a special case of functionalization [69, 70].

Covalent Functionalization Covalent functionalization can be implemented onto CNTs end caps or on their side walls that have numerous defects. Strategies for covalent functionalization are presented in Figure 1.4f [65]. Direct covalent side wall functionalization can be performed via reaction with particular molecules which possess high chemical reactivity. Initially, CNTs fluorination became popular due to the supposition that CNTs side walls are inert [71, 72]. CNTs that were functionalized via the fluorination method, possess weaker C—F bonds in comparison with alkyl fluorides [73]. Therefore, fluorinated CNTs provide replacement sites for additional functionalization [74]. Fluorine atoms substitutions by hydroxyl, alkyl, and amino groups were successfully achieved to date [75]. Plasma treatment can be utilized for MWNTs after functionalization. For example, maleic anhydride joint

with MWNTs after plasma treatment of the latter improves the obtained material mechanical properties as well as electrical conductivity [76]. Moreover, the grafting approach can be used to synthesize SWNTs which will possess high polymer layers covalent bonding density [77]. In [77] styrene copolymers benzyl chloride groups reacted with the SWNTs alkyne groups which lead to a greater efficiency of polymer chains grafting.

The chains of polymer grafting on the surface of CNTs are associated with the establishment of strong chemical bonds appeared between the nanotubes and polymer. Plasma treatment provides an increase in the CNTs ability to disperse when mixed with the corresponding polymer. Moreover, it increases structural properties if implemented in bulk composites. The drawback of this method consists in the limitation of grafted polymer value due to macromolecules high steric hindrance and comparatively low reactivity. It can result in degradation of nanocomposites features [78].

Noncovalent Functionalization Methods of chemical functionalization have two main disadvantages which consist in a creation of a huge defect number onto CNTs side walls as well as in some cases due to ultrasonication treatment, CNTs breakage into small pieces. These drawbacks lead to disruption of π-electron system in CNTs and significant deterioration in its mechanical and electrical properties. Physical functionalization overcomes these issues. This method is based on supramolecular chemistry [79]. It comprises van der Waals forces, electrostatic effects, hydrogen bonding, π–π interactions, ionic bonding, and hydrophobic forces [80]. The modeling of functionalization materials can be performed with the usage of density functional theory (DFT). Thus, CNTs functionalized with free-based tetraphenyl porphyrin molecules possess biding energies from 1.1 up to 1.8 eV and demonstrate a strong π–π interaction between CNT and tetraphenyl porphyrin surface [81]. CNTs solution with polymers like polystyrene, polyphenylene, polyvinylene result in the polymer wrapping around CNTs forming supermolecular CNTs complexes [82]. Surfactants are also very popular materials for CNTs functionalization [83–89]. Many studies were reported on nonionic surfactants like polyoxyethylene octyl phenyl ether, nonylphenol ethoxylate as well as polyoxyethylene 8 lauryl [83–85]. The nonionic surfactants treatment is grounded on a strong hydrophobic attraction between the tail group and the surfactant solid surface. After surfactant adsorption on the surface of the material for functionalization, the molecules of the surfactant are self-assembled in micelles beyond the critical micelle concentration [85]. Furthermore, researchers also investigated numerous anionic surfactants such as poly(styrene sulfate), sodium dodecylbenzene sulfonate, and sodium dodecylsulfate [86, 87]. Moreover, cationic surfactants like cetyltrimethylammounium 4-vinylbenzoate and dodecyl tri-methyl ammonium bromide were studied as well [88]. The mechanism of aggregates formation preventing is based on the lowering CNTs surface tension caused by surfactant physical absorption on the CNTs surface. By steric or electrostatic repulsive forces, CNTs treated with surfactants overcome the van der Waals attraction. This method effectiveness is influenced by the surfactants properties, polymer matrix as well as by medium chemistry [89].

Moreover, some researchers report a SWNT functionalization technique, which includes both physical and chemical approaches. For instance, in [90] scientists present cyanate ester (CE) reinforcement. Authors of this work used a dispersant hydroxyl polyimide-graft bisphenol to enable usage of the both above-mentioned functionalization methods. Then, epoxidized SWNTs were used with diglyceryl acrylate (PIOH-BDA). Thus, SWNTs were functionalized physically with the help of PIOH-BDA dispersant. This approach led to a better SWNTs dispersion due to the interaction caused by 1,4-butanediamine (BDA) side chain steric hindrance and the main chain. In addition, epoxidized SWNTs are also functionalized chemically by PIOH-BDA due to PIOH-BDA reaction with SWNTs epoxide groups and CE.

Applications of Functionalized CNTs Applications of functionalized CNTs cover many spheres of human life. Thus, in [91] researchers developed an immunosensor of voltammetric factor-alpha tumor necrosis (TNF-α). This sensor comprises Au nanoparticles included in functionalized with thiol MWNTs (AuNPs/S-MWCNTs) as well as bimetallic Ni/Cu-MOFs. AuNPs/S-MWNTs in this construction work as a platform for sensor when Ni/Cu-MOFs works as an amplifier of the sensor. First of all, a mixture of S-MWNTs and AuNPs was used to create the platform of the sensor on glassy carbon electrode. The sensor platform plays two roles in the device: enhancement in conductivity on the electrode surface and binding sites formation for capture antibody 1-TNF-α. After that, via amino-Au affinity, capture TNF-α antibodies were paired with the platform of the sensor. Then, through immune reaction that occurs between Ni/Cu-MOFs which are conjugated with secondary TNF-α antibodies and AuNPs/S-MWNTs, the immunosensor was created. Due to bimetallic MOFs' big internal surface and its porosity secondary antibody 2-TNF-α conjugate without difficulty to Ni/Cu-MOFs through electrostatic and π–π interactions leading to electrochemical performance improvement [92]. Such immunosensor possesses a small border of detection which is 2.00 fg ml^{-1} as well as a linear range that lies from 0.01 up to 1.0 pg ml^{-1} [91].

A membrane for desalination based on CNTs functionalized with polytetrafluoroethylene/oleic acid was developed in [93]. First, CNTs were functionalized with oleic acid. After that, the composite membrane was developed by solution coating of polyvinylidene fluoride that contains functionalized CNTs onto support membrane made from polytetrafluoroethylene. Polytetrafluoroethylene support membrane has hydrophobic pores that help to pass water vapor. The active layer coating of CNTs functionalized with polytetrafluoroethylene/oleic acid onto the polytetrafluoroethylene support membrane leads to an increase in salt rejection by about 30%. CNTs functionalized with oleic acid may decrease the oxidized CNTs hydrophilicity. The polyvinylidene fluoride polymer existence on the functionalized CNTs surface and between the CNTs improves the membrane quality of operation in the vacuum membrane distillation process and increases the membrane hydrophobicity. In contrast, the polyvinylidene fluoride polymer presence leads to the CNTs interconnection in the coated active layer. The optimum fabrication conditions consist in concentration of 10 000 ppm, temperature of 70 °C as well as the flow rate of 150 LPH (liters per hour). The membrane based on polytetrafluoroethylene/oleic

acid-functionalized CNTs composite allows to achieve high salt rejection of 99.45% as well as water flux of 89 LMH (liters per square meter per hour) in the vacuum membrane distillation process.

Moreover, functionalized SWNTs can be used for visible-light photocatalysis [94]. In [94] researchers performed endohedral functionalization of SWNTs with 10-phenylphenothiazine (PTH). The method used in this work is based on PTH solution refluxing in the cap-opened SWNTs presence. This technique made it possible to encapsulate inside the SWNTs as much as 8% of PTH. The obtained PTH/SWNTs structure demonstrates intense photoemission under visible light irradiation that makes it useful as a heterogeneous photocatalyst in reactions of single-electron transfer dehalogenation. Additionally, this material can be used for hydrodehalogenation reactions and more complex reactions like synthesis of tetrahydroisoquinolines as well as aldehydes α-alkylation when exposed to 420 nm light irradiation. This material possesses a high photocatalytic activity, showing turnover numbers of 3200. Furthermore, PTH/SWNTs structure demonstrates stability and recyclability. The physical process leading to these properties consists of the following. Under radiation exposure, an excited PTH electron is transported from the molecule π system to the delocalized SWNT π-cloud, therefore justifying the enhanced photocatalytic activity. Therefore, injection of electrons with subsequent electron–hole separation leads to the photocatalytic activity under visible light exposure, which initiates reactions of single-electron transfer dehalogenation.

MWNTs functionalized with pyrene derivatives comprising a hydroxyl group can be utilized as a polybutylene terephthalate (PBT) composites filler [95]. In [95] researchers physically functionalized MWNTs with 1-hydroxypyrene (POH), 1-pyrenebutanol (PBOH), as well as with 1-pyrenemethanol (PMOH). Then, functionalized MWNTs are used for compound fabrication with PBT with the help of melt extrusion. In the process of extrusion, a transesterification reaction appears between the PBOH hydroxyl group and PBT ester group, thus grafting PBT onto MWNTs. Because of the most stable intermediate formation as well as the minimum change in free energy at the rate-determining step for PBOH, the PBT reactivity turned out to be greater with PBOH than with PMOH or POH, which was proved via density functional theory calculations. Due to the same reason, the biggest grafted PBT amount can be observed in the structure PBOH-MWNTs. Estimated energies of interfacial adhesion between MWNTs and PBT showed that the PBOH-MWNTs structure possesses greater interfacial adhesion energy with PBT than MWNTs functionalized with POH or POMH. In addition, the structure PBT/PBOH-MWNT demonstrates the maximum fatigue life tensile property as well as tensile property between the presented composites.

Functionalized CNTs can be used as selective and highly sensitive elements of photodetectors and light-harvesting devices [96–99]. In [96] researchers developed a tunable photodetector based on SWNTs functionalized with pyrenecyclodextrin. They build a field-effect transistor (FET) based on the synthesized material in order to detect a fluorescent adamantyl-modified Ru complex (ADA-Ru). Under light irradiation of 280 nm wavelength, the obtained photodetector transfer curve shifts to a negative gate voltage by approximately 1.6 V as well as the aforementioned

device conductivity decreases sharply, signifying a charge-transfer process to the SWNTs from pyrenecyclodextrins. On the other hand, the photodetector transfer curve shifts to a positive gate voltage by approximately 1.9 V and its conductivity growths slowly under 490 nm light exposure when ADA-Ru complex is introduced in the system. It also demonstrates a charge-transfer process, but at that time it goes from pyrenecyclodextrin-SWNT hybrids toward the ADA-Ru complex. As soon as the radiation exposure is turned off, the conductivity volume recovers to its initial value.

In [97] researchers developed a NIR–photodetector based on functionalized with ferricyanide SWNTs. It was demonstrated that SWNTs functionalized with quite big diameter molecules of ferricyanide show the change in emission and photo-absorption in the same CNT simultaneously. It is caused by partial electron transfer which vanishes the optical transition and localizes electrons. The ferricyanide can be reduced by hydrogen peroxide that will reverse the occurred electron transfer, which leads to a re-establishment of emission and absorption spectra. The selectivity of such device manifests itself in the form of different absorption that leads to a higher response with smaller gap species. In [98] researchers functionalized SWNTs with CdS. They developed a CdS-SWNTs film-based device with two terminals. Initially, researchers intended to develop solar cells based on functionalized CNTs but they also observed its behavior under light exposure that demonstrates its applicability in visible light photodetectors. This device shows current flow increase under light irradiation. The change of current saturates in approximately 30 seconds under light exposure. In [99] a tunable photodetector based on functionalized SWNTs was developed. SWNTs were functionalized with ZnO nanoparticles that were utilized as antennas in this structure. The improved responsivity of as-prepared device refers to the synergistic effects of the inherent SWNTs transistors sensitivity as weak as the ZnO nanoparticles photoresponsivity occurring from the zero dimensionality materials nature and the big surface-to-volume ratio.

The photodetector demonstrates significant photoswitching effects with decent reproducibility and reversibility because of photoinduced oxygen desorption as well as adsorption from the surface of nanoparticles. The photodetector under consideration possesses fine conductance tunability in the range of UV light spectrum. Such devices can be utilized in various applications like imaging, UV detection, optical communications, and memory storage.

CNTs are a very useful material for development of gas and molecule sensors [100–105]. Thus, in [100] researchers used covalently functionalized SWNTs as a sensitive element for ammonia detectors. Researchers functionalized SWNTs with poly(*m*-aminobenzene sulfonic acid) (PABS). SWNTs-PABS detector fast recovers its conductivity when ammonia is replaced with nitrogen. When NH_3 is supplied to the detector, significant changes occur in the SWNTs-PABS structure. Due to this fact, such detector can detect 5 ppm concentration of NH_3. In [101] alcohol vapor detectors based on covalently functionalized MWNTs were developed. Construction of this detector includes bundles of functionalized MWNTs with COOH groups deposited across golden electrodes on SiO_2/Si substrate with the help of AC

electrophoresis. This structure allows to detect alcohol–vapor with the usage of low input power of approximately 0.01–1 μW. This detector possesses a sensitivity of 0.9 ppm alcohol–vapor concentration. Moreover, this detector can be reset by annealing the functionalized MWNTs sensitive element at a current from 100 up to 200 A in a time duration of 100–200 seconds. A chloroform vapor detector based on covalently functionalized MWNTs with COOH with poly(ethylene glycol) (PEG) was developed in [102]. Selective response of the structure can be explained via PEG chains swelling behavior wrapped around MWNTs and the interaction among PEG chains, MWNTs, as well as analytes, might be a vital factor in the sensing of gases. The change in conductivity of films occurs due to the change in intertube distance caused by polymer swelling through gas absorption. In contrast, the MWNTs-g-PEG film response to chloroform is different from the response to other solvents that are referred to hydrogen bond interaction between PEG chains and solvent molecules. MWNTs features significantly affect this interaction. Moreover, CNTs can be utilized as hydrogen gas sensors [103–105]. Hydrogen gas detector based on functionalized MWNTs with acids was investigated in [103]. Such sensor can allow detecting H_2 gas in a quantity of 0.05% at room temperature. In comparison with pristine MWNTs, MWNTs functionalized with acids possess increase in the current carrying capacity up to 35 mA from 49 μA and smaller recovery time which is 100 seconds for H_2 gas in a quantity of 0.05% compared with 190 seconds in case of pristine MWNTs. In addition, MWNTs functionalized with oxygen plasma can be used as a gas sensor for such volatile organic composites as ethanol, acetone, toluene, benzene, as well as methanol [105]. The conductivity of the functionalized MWNTs decreases with the increase of detecting vapor concentration. Such sensors possess repeatable response and reproducibility in case of benzene or toluene vapor. Methanol, acetone, and ethanol show faster response coupled with difficulties in a full baseline resistance recovery. It can be referred as the chemisorption interaction mechanism with MWNTs. In contrast, toluene and benzene are physisorbed onto MWNTs that causes fully baseline resistance recovering and slower response. It is demonstrated that MWNTs detectors are more sensitive to toluene than to benzene vapor. It can be caused by the methyl group existence in the toluene molecule that interacts better with MWNTs sidewalls than the benzene ring. This structure feature allows to develop detectors that will detect benzene selectively in the presence of xylenes or toluene with the usage of plasma-treated MWNTs functionalized with different metals or functional groups arrays chemoresistors.

1.2.4.8 Applications of CNTs

As mentioned above, the peculiar, strong and powerful optical, electronic, mechanical, as well as chemical properties, make CNTs useful in innumerable applications. In the current decade, CNTs have become a hot material for electronic, chemical, mechanical, and optical applications. Due to their excellent electronic properties, CNTs allow the fabrication of basic solid-state devices with smaller dimensions than conventional silicon-based technology. Recently developed basic electronic devices based on CNTs are diode, tunnel diode, FETs, and supercapacitors. It is also successfully used in the fabrication of devices in some other important applications:

microwave amplifier, flat panel display, radio, X-ray source, random-access memory (RAM) as well transparent conductor [106–108]. CNTs have also been used in very important communications and information technology inventions such as fiber lasers and nonlinear photonics. These inventions play a role in routing, wavelength conversion, and optical switching. It is also used in applications such as photovoltaic devices, photodetectors, and nano-light sources [109–111].

CNTs have also proven to be a promising future material in the field of mechanical applications. Worldwide researchers are working on nano electro mechanical system (NEMS) technology based on CNTs. Researchers have successfully developed mechanical devices based on high-frequency oscillators [112], rotational actuators [113], nanometer tweezers [114], and nanometer cargoes [115]. Outstanding inventions are ultra-miniature sensors for observing the working force between two molecules [116], for measuring the force produced by the magnetic resonance of a single spin [117], and for measuring the displacement created by disturbance between individual atoms. Due to their relatively high Young's modulus as well as specific weight, SWNTs have proved to be perfect for manufacturing mechanical resonators for observing mechanical movement in the quantum regime [118].

CNTs have also been part of surprising inventions in the field of electrochemistry. Several types of chemical sensors, humidity sensors, gas sensors for toxic gases, and alcohol sensors are developed so far. CNTs-based chemical sensors have the following advantages over conventional solid-state sensors.

I. Existing sensors show poor sensitivity at room temperature. Their normal operating temperature is in the range of 200–500 °C. However, CNTs-based sensors work successfully at room temperature.
II. Existing toxic gas sensors show a limited maximum sensitivity in comparison with CNTs-based sensors that have shown order of magnitude higher sensitivities.
III. The main drawback of using oxide-based gas sensors is the use of microfabrication techniques to build the sensor that puts a limit on the size and geometry of the sensor. In the case of CNTs, due to their small dimensions, no barrier is created in front of the device design and geometry.
IV. For existing technology, the sensor fabrication cost is very high compared to CNTs-based sensors.
V. The operating power of existing sensors is also very high. It is possible to operate CNTs-based sensors at very low power.
VI. Existing toxic gas sensors show very poor selectivity. They possess nonspecific gas sensing mechanism and very poor response time. These problems are resolved with CNTs-based sensor technology.

1.2.4.9 Synthesis of CNTs

In order to develop a material with specific properties, it becomes most important to be aware of all the growth techniques so that it becomes possible to synthesize material with the best quality and yield. There are three main techniques used to grow CNTs: arc discharge, laser ablation, and CVD. Amongst them, CVD is the most used technique so far.

Arc Discharge Method Arc discharge method is a widely used method for CNTs growth. It was invented by Krätschmer et al. to produce a high yield of fullerenes [119]. It was observed that in addition to fullerenes, some other allotropes of carbon were also present as by-products. Later, a microscopist Sumio Iijima reported the presence of tubular allotrope of carbon, i.e. CNTs, in the arc discharge method by-products [120]. Therefore, arc discharge was the first known method for the CNTs growth. This method was further developed and optimized for exclusive CNTs growth. Initially, the synthesis of CNTs in the soot form using this method was reported [120].

Earlier, only MWNTs were produced using this method, but at the later stage, it has been successfully tuned for the growth of SWNTs [121]. The arc discharge method involves the vaporization of graphite in an inert atmosphere using an electric arc. In specific cases, catalysts also take part in the synthesis of CNTs. At the heart of the arc discharge system, there are two graphite rods situated inside the electric arc chamber. The diameters of graphite rods are of the order of 2 mm and the separation between these rods is kept about 1 mm (see Figure 1.5a). These graphite rods act as electrodes and a high DC current of around 50–100 A is passed through them. Due to such high DC current, a very large amount of thermal energy is produced, which increases the temperature of the system up to around 4000 °C, which, in turn, evaporates the carbon of the graphite anode. These carbon vapors subsequently deposit on a cathode in the form of different carbon nanostructures such as CNTs, fullerenes, and amorphous carbon [122–125]. The electrodes composition determines the type and quality of as-synthesized CNTs among the grown carbon nanostructures [126]. While pure graphite electrodes support the synthesis of MWNTs, SWNTs can be produced using graphite electrodes mixed with metal catalysts [119, 127]. Another property of as-grown CNTs is their diameter, which can be tuned by controlling other growth parameters [123].

Laser Ablation The laser ablation method is quite similar to the arc discharge method. In both techniques, carbon is vaporized and deposited at different places. The only difference in both growth methods is the evaporation process. In the laser ablation technique, a high-intensity laser beam is used for carbon vaporization instead of high DC current. A small amount of carbon is transmitted into its plasma. CNTs with other allotropes of carbon are synthesized into a plasma plume. The plasma plume subsequently deposits on the chamber walls. This technique mainly uses CO_2 and Nd:YAG laser sources in both pulsed and continuous modes [128, 129]. This method, like the arc discharge technique, can be used to deposit both MWNTs and SWNTs. When pure carbon source is used, the growth of MWNTs takes place. On the other hand, the use of metal catalyst mixed carbon source leads to the synthesis of a mixture of MWNTs and SWNTs. Figure 1.5b shows a schematic diagram of the laser equipment.

Chemical Vapor Deposition The CVD system is basically a film depositing equipment that has been used for many years and is capable of depositing a number of nanomaterials. CVD is a method in which gaseous precursors react either in the gas phase or

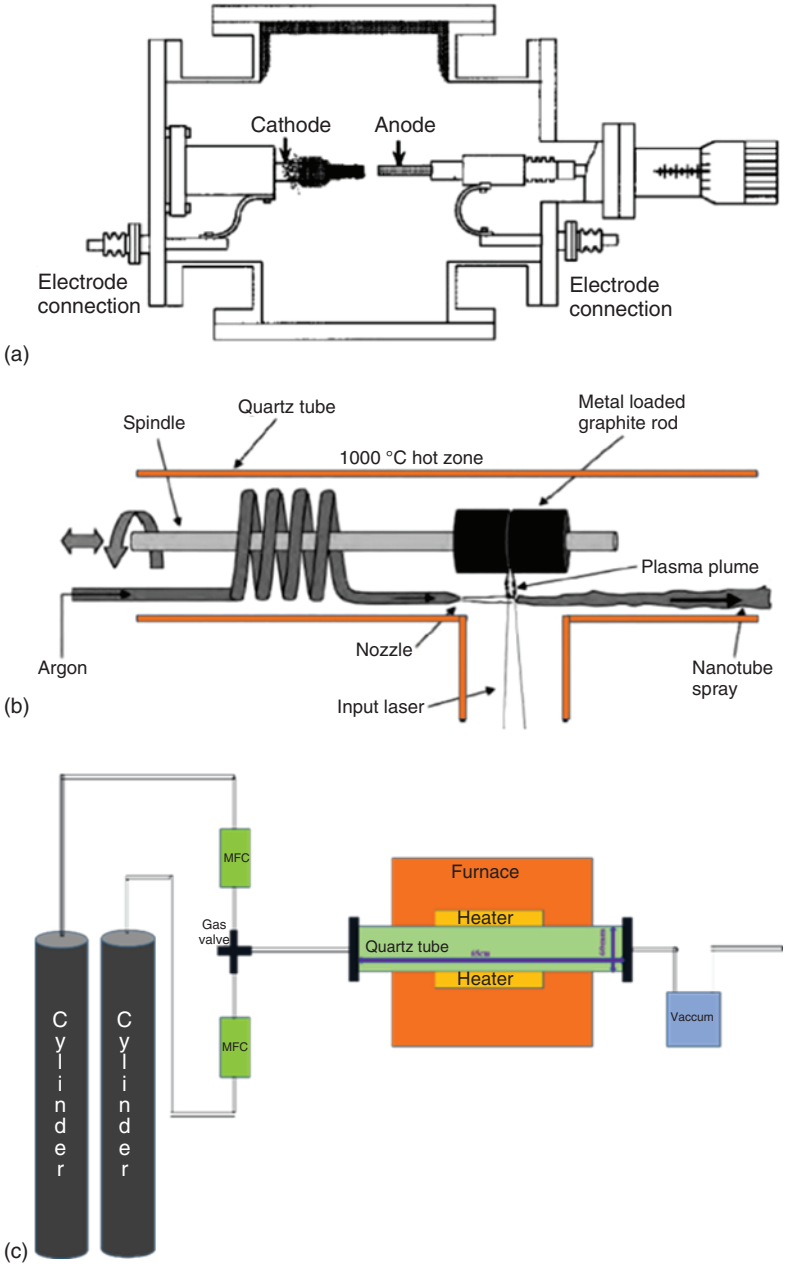

Figure 1.5 Figure (a–c) show the schematic diagram of arc-discharge, laser ablation, and CVD techniques. Source: Saito et al. [122]/with permission of AIP Publishing.

at the substrate gas interface, producing a thin film on the substrate. In the research world, there are many types of CVD systems having various types of heating arrangements as well as some extra accessories. Atypical thermal chemical vapor deposition (TCVD) setup includes a durable, high-temperature compatible tube, usually made of quartz or alumina, which is heated by a chamber furnace or heating coils (see Figure 1.5c).

All types of CVDs have the same operating concept. Users customize CVD according to requirements. Thermal and plasma enhanced CVDs are being used to fabricate CNTs. The CNTs growth by the CVD process requires three ingredients: anablation precursor gas (also called feedstock), a catalyst surface, and an energy source. Energy may be generated thermally (in TCVD) or by plasma (in plasma enhanced CVD). We preferred using TCVD for CNTs growth (since CNTs are prone to be damaged by plasma [130], which reduces their electrical performance). In TCVD, hydrocarbons are broken at high temperatures to produce atomic carbon vapors. These vapors are deposited on the metal catalyst deposited substrate via vapor–liquid–solid (V–L–S) growth process to form CNTs. The V–L–S growth process involves three steps, i.e. absorption, saturation, and structure extrusion (see Figure 1.6a). Any transition metal that has a low melting point can be used as a seed or catalyst for CNTs growth via the V–L–S growth process. These catalysts have the ability to absorb vaporized carbon [131–133]. These catalysts may be deposited on a substrate such as silicon, Al_2O_3, etc. in the form of thin film by sputtering, dip coating, or spin coating. Prior to deposition, the catalyst-coated substrate is heated. Because of heat treatment, the continuous layer breaks into lumps of nanoparticles to keep minimum surface energy.

This process is known as catalyst activation or annealing. In some reports, catalysts were injected directly into the growth chamber. Some oxide nanoparticles (SiO_2, Al_2O_3) have also been reported as catalysts for CNTs growth [2]. After putting the annealed catalyst film into the chamber, the chamber is evacuated. The precursor gas, which is usually a lower-order hydrocarbon (such as methane, acetylene, and ethylene), is then introduced into the chamber at an appropriate pressure. In some specific cases, vaporized benzene or toluene can be used as a feedstock. Occasionally, an inert carrier gas is also used as a carrier, which also serves as an etchant for excess amorphous carbon deposited on the walls of the chamber. The chamber temperature is raised to several hundred degrees Celsius. Such a high temperature induces the metal catalysts nanoparticles to get into a molten state. On the other hand, high temperature also decomposes hydrocarbon. Decomposition of hydrocarbons produces carbon vapor in the chamber, which is absorbed by the molten catalyst. As more and more carbon is absorbed by the catalyst, the concentration of carbon exceeds the solubility of the catalyst particle. At this point, the catalyst particle begins to extrude a solid formation in the form of a CNT as shown in Figure 1.6a,b. The schematic diagram of CNTs growth via V–L–S process is given in Figure 1.6. Depending on the final location of the catalyst particle, nanotubes are typically classified as either tip-grown or root-grown. Other one-dimension nanostructures can also be grown via V–L–S growth mechanism. The growth of germanium nanowires from gold nanoparticle is shown in Figure 1.6c–i, and the growth

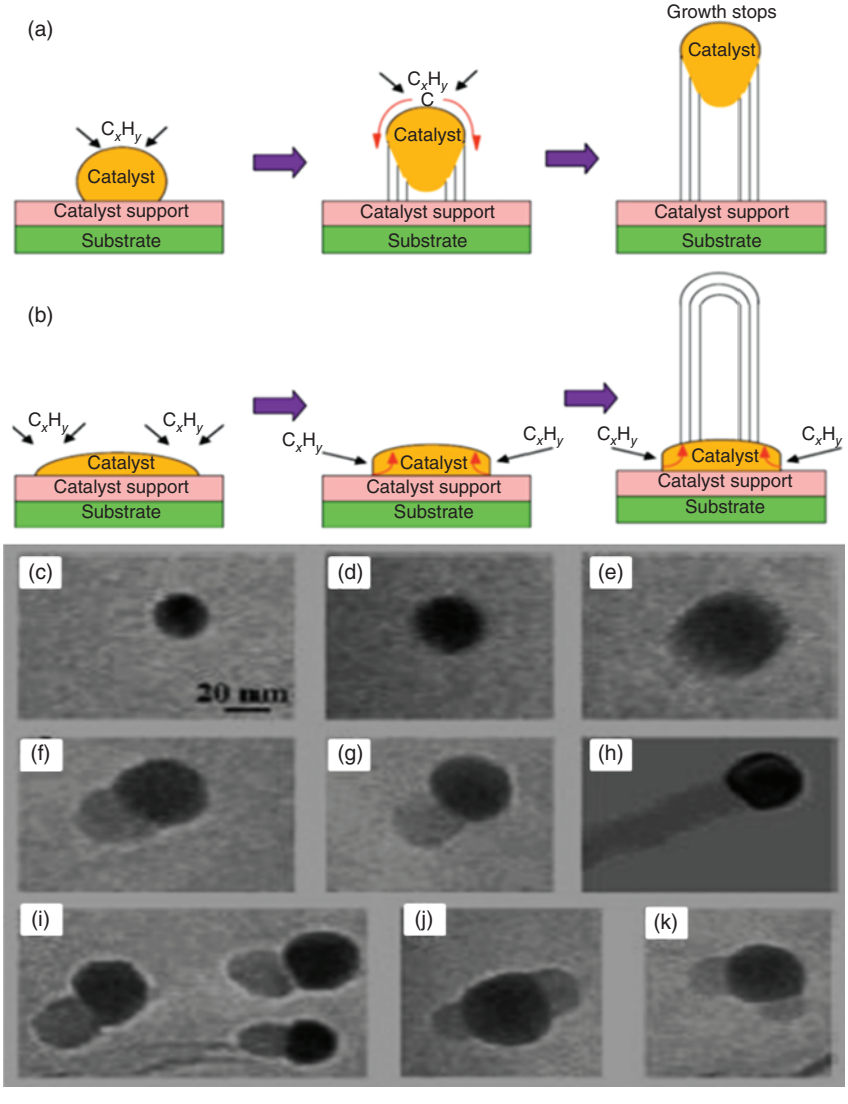

Figure 1.6 Schematic diagram of various stages of V–L–S growth mechanism. Figure (a) represent the tip-growth model while figure (b) shows the base growth model. Source: Sengupta [131]/with permission of Elsevier. Figure (c–k) shows the formation of germanium nanowires from gold nanoparticles via the vapor liquid solid growth mechanism. These transmission electron microscopy images reveal the extrusion of the germanium nanowires (e–k) from the saturated particle (c, d). Source: Wu et al. [131]/ with permission of American Chemical Society.

of multiple nanowires is shown in Figure 1.6j,k. The major benefit of using CVD for the synthesis of CNTs lies in its ability to be scaled up in size, allowing the large production facilities to produce several kilograms of CNTs per day [134].

Hydrocarbons are channeled into the heated reactor zone via mass flow controllers and eventual by-products are evacuated through a fume hood. TCVD can

be used to grow MWNTs as well as SWNTs. CVD parameters such as temperature, pressure, flow of gases, etc. play a crucial role in deciding CNTs dimensions, structure as well as quality [135, 136]. They have varying degrees of interaction with growth conditions, which is further complicated by the fact that different research results often predict different behavior. All this makes it a quite challenging task to find out the optimum growth conditions for producing CNTs with desired properties. Now, after gaining knowledge about the CVD system, a detailed analysis of the various parameters used in the CVD system has become necessary. Therefore, now we are going to present a detailed literature survey on various CVD parameters.

CNT Precursors In the CVD system for growing CNTs, the most commonly used carbon feedstock compounds are methane (CH_4), ethylene (C_2H_4), acetylene (C_2H_2), benzene (C_6H_6), xylene (C_8H_{10}) as well as carbon monoxide [130, 137–141]. The CNTs growth by pyrolysis of benzene was reported at 1100 °C [142, 143], while MWNTs with an acetylene precursor had been grown at 700 °C [144]. In both cases, benzene and acetylene, iron catalysts are used for hydrocarbon decomposition. Later, cyclohexane (C_6H_{12}) and fullerene were also successfully tested as precursors for CNTs growth [145–147]. If we are talking about SWNTs, H. Dai et al. first reported about SWNTs growth using carbon monoxide as a carbon precursor and molybdenum as a catalyst while keeping the growth temperature at 1200 °C [148]. After H. Dai et al. made a milestone report on SWNTs synthesis, many other groups also became succeeding SWNTs growth with different carbon precursors, such as acetylene [149], methane [150], and benzene [151], etc. with various catalysts. A report of Maruyama et al. (2012) introduced a new carbon precursor, i.e. alcohol for SWNTs growth [152]. They grew high-quality SWNTs at a lower growth temperature on zeolite-supported Fe–Co nanoparticles. Due to its extraordinary qualities, alcohol became the highest used hydrocarbon source for SWNTs synthesis [153, 154]. It is reported that due to the carbon etching ability of alcohol, CNTs grown with alcohol precursors have a lesser amount of amorphous carbon [155]. After some time, the same group also synthesized vertically aligned SWNTs on a quartz substrate using Mo-Co catalyst with an alcohol precursor [156]. Maruyama et al. also enhanced the catalytic quality of the catalyst by using a discontinuous flow of acetylene in an ethanol-based CVD and increased the growth rate of CNTs [157]. The structural formation of the hydrocarbon source has the potential to decide the CNTs structure. Linear carbon precursors like acetylene, ethylene, and methane produced straight and hollow tubes, while benzene and cyclohexane-type cyclic hydrocarbons produced curved CNTs [147]. Generally, MWNTs synthesis is easy as compared to SWNTs. Moreover, MWNTs grow at lower temperatures as compared to SWNTs. One more observation is that MWNTs can grow with any precursor while SWNTs growth takes place on selective precursors. Common carbon precursors used for MWNTs synthesis show unstable behavior at higher temperatures. It leads to the synthesis of other carbonaceous compounds instead of CNTs. To solve that problem, in 2004 Hata et al. published a report, in which water-assisted CVD is proposed to grow impurity-less SWNTs. In water-assisted

CVD, water steam is supplied in a controlled manner as an oxidizer. It etches out amorphous carbon without damaging the grown SWNTs [158]. Another work is reported by Zhong et al., in which they proved that no water steam type oxidant is required in cold wall CVD systems. It is successful only for low reactive carbon precursors [159]. The above discussions emphatically show that hydrocarbon or carbon precursors have an important role in CNTs growth. Therefore, researchers get the best yield as well as structure of grown CNTs by proper tuning and selection of carbon precursors.

Apart from the types of hydrocarbons, the flow rate and flow duration of hydrocarbons also play an important role in CNTs growth by TCVD. To analyze the various effects of hydrocarbon flow rate and flow duration, we performed several experiments with different flow rates (10–50 sccm) and flow duration (2–16 minutes) of C_2H_2while keeping other parameters of the CVD system constant. It has been observed that initially the structural quality of CNTs enhanced with an increment of C_2H_2 flow rate and, after a certain limit of C_2H_2 flow rate the structural quality of CNTs starts to degrade. The best quality of CNTs has been grown at a 12 sccm flow rate of C_2H_2. Similarly, in case of C_2H_2 flow duration, the quality of CNTs has been enhanced when we increased flow duration from 2 to 12 minutes, but beyond this limit structural quality of CNTs started to degrade. The best quality of CNTs has been found with 12 minutes flow duration of C_2H_2 [136].

Catalyst Engineering As we discussed earlier, for CNTs growth nano-scale particles are needed to trigger the carbon precursor decomposition at a lesser temperature than its actual decomposition temperature as well as to initiate CNTs growth. In the early time of CNTs invention, transition metals (Fe, Co, Ni) were used as catalysts for CNTs growth. Due to high solubility as well as high carbon diffusion rate of transition metals, they are preferable in CNTs growth. High melting point and low equilibrium vapor pressure of transition metals also give a large range for selecting growth temperature as well as a large number of carbon precursors. It is also reported by some groups that transition metals have better adhesion with grown nanotubes compared to other metals. That quality of transition metals provides grown CNTs with large curvature and lower diameter [160]. Some reports also made evidence of solid organometallic precursors having quality of catalyzed CNTs indeed better than transition metals. Apart from Fe, Co, and Ni, some other metals such as Pd, Pt, Cu, and Au also have the potential to catalyze CNTs with different carbon feedstock [161]. Generally, a tube diameter depends very much on the catalyst particles' size [147]. Some groups manipulate the size of catalyst particles prior to growth and hence the diameter of CNTs [162]. To get pure nanotubes, it is necessary that carbon precursors used in CNTs growth decompose only on catalyst particles and avoid aerial pyrolysis. As mentioned previously, metal catalysts are also used in arc discharge as well as laser ablation techniques of growth CNTs, so it may be possible that these different techniques have the same growth mechanism.

It has been observed that metal salts such as iron nitrate, magnesium nitrate, cobalt nitrate, etc. can be also utilized as catalysts for growing CNTs. The density and orientation of CNTs can be tuned by selecting the appropriate metal salt as a

catalyst. It has been observed that cobalt nitrate and magnesium nitrate are capable to produce horizontal network type CNTs with acceptable structural quality. The CNTs density is much higher in the case of magnesium nitrate as compared to cobalt nitrate. In case of iron nitrate, vertically aligned CNTs have taken place when iron nitrate was used as a catalyst. Therefore, by utilizing different metal salts, someone can tune the yield as well as orientation of CNTs. Vertically aligned CNTs can be also produced by oxygen plasma treatment of catalyst film prior to CNTs growth. Oxygen plasma treatment enhances the nucleation sites on catalyst particles. Hence, the density of CNTs sharply increases and due to crowding effect vertically aligned CNTs grow [1]. The height of CNTs is another important requirement for application development. It has been observed that the flow rate of carrier gas is affecting significantly on CNTs height/length. We performed several experiments on CNTs synthesis at different argon flow rates (0–80 sccm). Initially, without argon gas very short length (~2 μm) CNTs growth took place but the height of CNTs increased sharply (~57 μm) when argon flow turned on 20 sccm flow rate. The height of CNTs is found varying as a function of the argon flow rate. In case of structural quality and diameter of CNTs, it has been found that they are improving up to 60 sccm flow rate of argon; beyond this limit, the diameter starts to increase and structural quality starts to degrade. Carrier gas increases the distribution of hydrocarbons inside the chamber, balances the production of carbon atoms and, as per requirement, grows CNTs. The best structural quality, less diameter, and acceptable height have been found at 60 sccm argon flow rate [5]. In the general CNTs growth mechanism, catalyst nanoparticles either remain on the bottom of CNTs or they peeled-off from the substrate and come on the CNTs tip. If the catalyst remains on the bottom of CNTs then it is called base-growth and when the catalyst particles come on tip then it is called tip-growth. It has also been observed that sometimes these catalyst particles remain inside CNTs. Many researchers reported that CNTs growth with a metal catalyst is not suitable for electronics, optoelectronics, medical, and agriculture applications. The metal catalyst is very harmful for all living organisms as well as for solid state devices [163]. Although metal catalysts can be removed from CNTs by performing certain post-growth purification processes, these processes are very complex and also create defects in CNTs. To solve this issue, many research groups tried to grow CNTs without catalyst as well as without metal catalyst [163–165]. To make CNTs more useful for mentioned applications, in our group we have grown CNTs without catalyst directly on Al_2O_3 substrate as well as by using green catalyst [2, 163]. It has been reported that Al_2O_2 is capable to decompose hydrocarbons at lower temperatures, and surface roughness of Al_2O_3 substrate provides nucleation sites for CNTs growth. The as-grown CNTs were few walls CNTs having diameters in the range of 4–8 nm and very high structural quality (see Figure 1.7a,b).

We also tried unconventional catalysts for growing CNTs, i.e. green catalysts. The walnut plant extract has been utilized as a green catalyst. Green catalysts are found able to grow CNTs at lower temperatures. To grow CNTs by using metal catalyst, generally 800 °C temperature is required but in case of green catalysts, CNTs growth took place at 575 °C. When CNTs growth performed at 800 °C, then a new carbon nanostructure with rectangular cross section took place (see

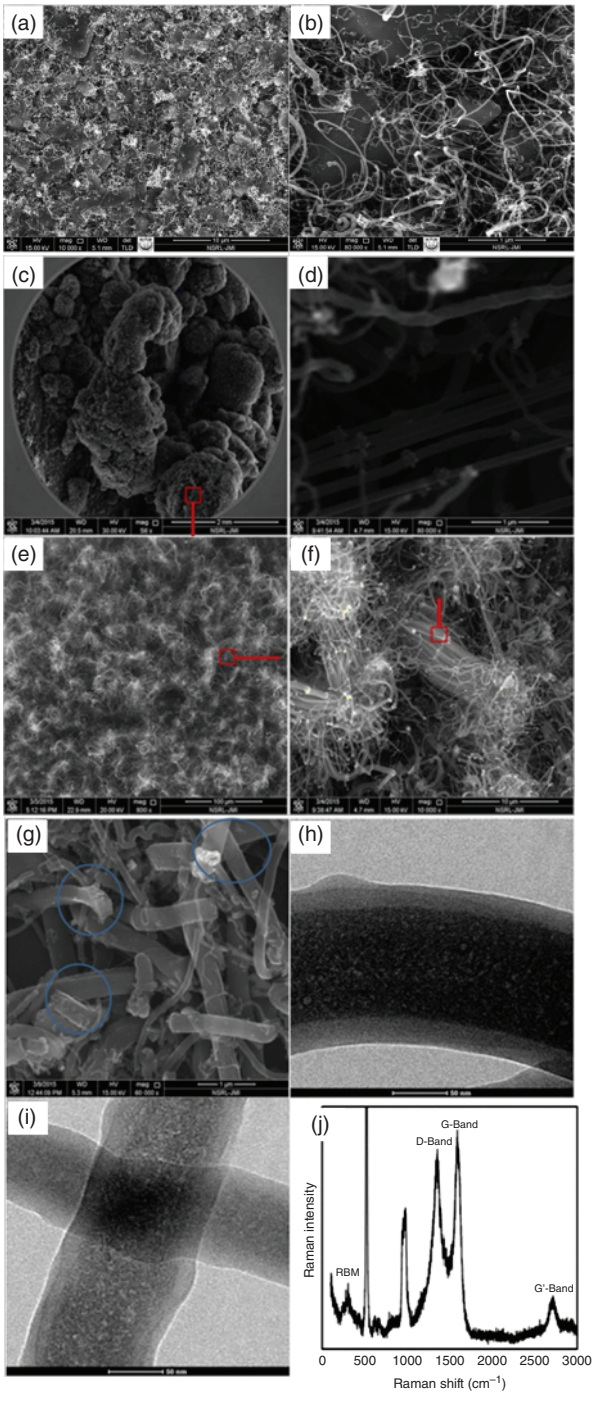

Figure 1.7 Figure (a) shows the FE-SEM image of CNTs growing on the Al_2O_3 substrate, its magnified image can be seen in figure (b). Source: Tripathi et al. [2]/with permission of Elsevier. Figure (c) shows CNTs growth by using green catalyst and its magnification image can be seen in figure (d–f). Figure (g) shows the carbon nanostructure with rectangular cross-section and figure (h, i) show TEM images of the as-grown nanostructure. Figure (j) shows its Raman analysis. Source: Tripathi et al. [163] / With permission of Springer Nature / CC BY 4.0.

Figure 1.7c–j). Apart from low temperatures growth, green catalysts are capable of growing CNTs on mass scale.

To verify the fact that only walnut plant extract can catalyzed CNTs growth or any plant extract, the CNTs growth has been performed by using *Azadirachta indica*, *Cascabela thevetia*, rose flower, and garden grass extract as catalysts. It has been observed that all mentioned plants are able to grow CNTs. Green catalyst finished the requirement of complex instruments, which required metal catalyst deposition. Since CNTs growth is conducted at low temperatures and green catalysts available freely in nature, all mentioned factors reduced the cost for CNTs producing [163]. Another important parameter of CNTs growth is the growth temperature and temperature increasing rate. The growth temperature and temperature increasing rate make a direct impact on catalyst particles and on the CNTs morphology and structural quality. We analyzed CNTs growth by performing multiple experiments by taking different growth temperatures (650–850 °C). At 650 °C growth temperature, obtained CNTs had a very poor structural quality and a large diameter. The structural quality/diameter of CNTs started to improve/decrease with rising growth temperature. The best structural quality with lesser diameter CNTs was obtained at 775 °C growth temperature. When the growth temperature further increased the structural quality/diameter started to decrease/increase. At a lower growth temperature, the catalyst film made large diameter catalyst particles. When the growth temperature increased, the diameter of catalyst particles has been found decreasing. After a certain limit of the growth temperature, the catalyst particles started to agglomerate and converted into larger size particles that is the possible reason for growth temperature dependent CNTs growth. Similar to the growth temperature, the temperature increasing rate makes a big impact on the CNTs structural quality as well as on the diameter of as-grown CNTs.

To analyze the various effects of the temperature increasing rate on CNTs growth, multiple experiments with different temperature increasing rates (from 100 to 600 °C per hour) have been performed. As explained earlier, when the catalyst film deposited sample is annealed in the presence of argon gas, the catalyst film is converted into nanosized hemispherical particles. It happened due to different thermal expansion coefficients of a metal catalyst film and a substrate. When the CVD temperature slowly increased, the catalyst film and substrate got sufficient time to balance thermal expansion rates. In that case, large size catalyst particles were produced. Opposite to this, when the sample was heated with a fast temperature increasing rate, the catalyst film has been broken into small size particles because of a large thermal expansion gradient created between the substrate and catalyst film. Also, when the sample was heated at a fast temperature increasing rate, lots of defects were created on catalyst particles and as-produced defects provided small size nucleation sites for CNTs growth. When CNTs growth experiment was conducted with 100°C per hour temperature increasing rate, large size poor structural quality CNTs were grown. The structural quality/diameter/no. of walls has been found increasing/decreasing/decreasing with respect to the temperature increasing rate increment. The best quality CNTs with a single wall have been grown at 600 °C per hour temperature increasing rate (see Figure 1.8) [166].

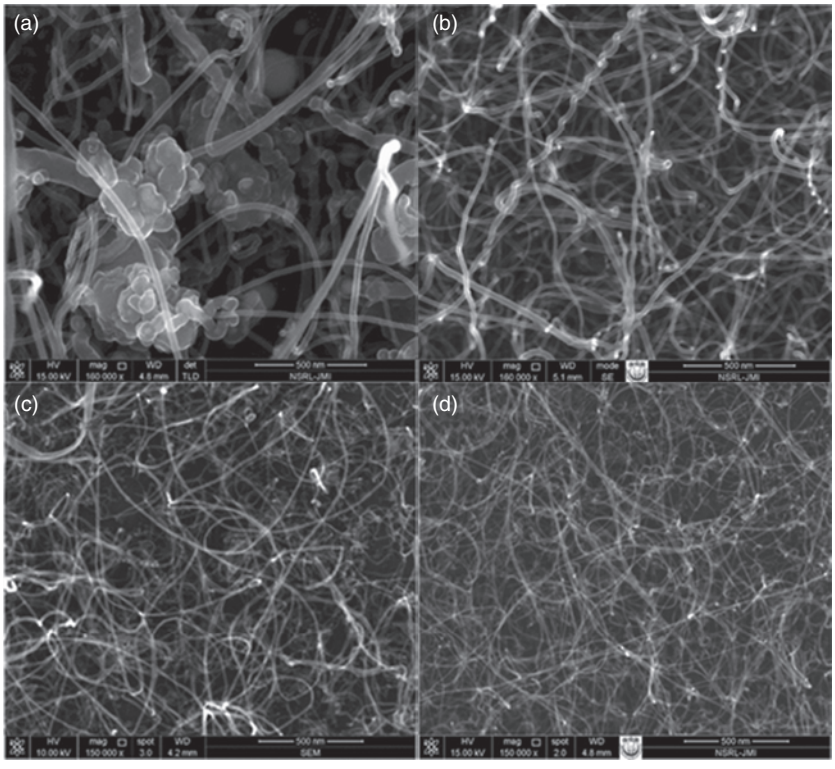

Figure 1.8 Figure shows the SEM monographs for as-grown CNTs with taking temperature increasing rate as (a) 100, (b) 300, (c) 500, and (d) 600 °C per hour, respectively. Source: Tripathi et al. [166]/with permission of Springer Nature/CC BY 4.0.

1.2.4.10 Analysis of CNTs by Raman Spectroscopy

Raman spectroscopy is one of the main tools used for molecular vibrations investigation. It is utilized to gain knowledge about chemical elements and structural forms to recognize materials by characteristic fingerprinting. It is also used to get quantitative information about the amount of material in a sample. This equipment has the potential of scanning samples in all states as well as in all conditions; for example, powder, vapors or liquids, surface layers, or bulk form of nanoparticles, in different temperature states. Prior, IR absorption was widely used as compared to Raman scattering (RS) due to complexity in Raman spectroscopy. But improvements in technology made Raman spectroscopy simple, compact and reduced the problems substantially. Mentioned improvements in Raman spectroscopy along with the capability of investigation of different type of samples without any preparation, make Raman spectroscopy a powerful investigation tool in the field of materials science. In 1928, Sir C.V. Raman reported the historical invention of inelastic light scattering. Raman scattering (RS) is defined as inelastic scattering of light. In inelastic scattering, the photon energy shifted with respect to the incident energy (see Figure 1.9a). The schematic diagram of the experiment is displayed in Figure 1.9b. In a basic concept, a laser beam is incident on materials, and the properties of scattered light

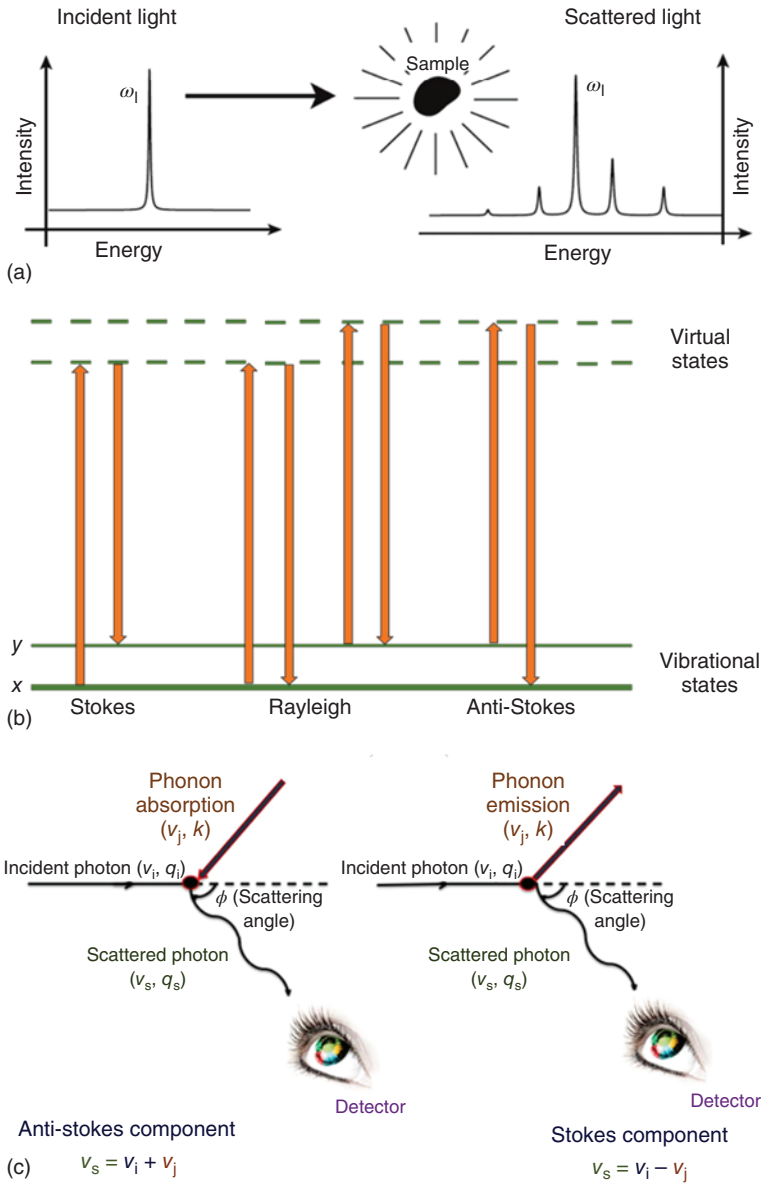

Figure 1.9 Figure (a) shows the phenomenon for Raman Scattering. Plot of figure (b) shows the sample identification and phase quantification Figure (c) shows the interaction mechanism that causes a frequency change.

from material is analyzed. Raman spectroscopy is known as a powerful and non-destructive tool that can rapidly give information about the low-frequency modes of materials along with rotational as well as vibrational modes [167–169]. Raman scattering phenomenon depends on the frequency change of photons after interaction with materials and such type of light–matter interaction is known as inelastic

interaction. If frequencies of incident and scattered photons are found to be the same, then such type of light-matter interaction is known as elastic scattering.

In RS, the atomic bond structure of materials is analyzed via inelastic interaction of incident light with the help of longitudinal/transverse modes of phonon. Spectral characteristics of phonon vibrations in solids can be investigated by RS. RS provides the platform for materials identification as well as phase quantification. The shift in frequency produced by light–matter interaction is displayed in Figure 1.9c. If the incident photon energy increase after the interaction by absorbing a phonon then the energy of scattered photons will also be increased and this process is called anti-Stokes Raman scattering. Opposite to anti-Stokes, if an incident photon reduces energy after the interaction by emitting a phonon, then the frequency of scattered photons will also be reduced, this phenomenon is called Stokes Raman scattering. It has been observed that in Raman spectra, generally, only Stokes peaks appeared. It happened due to the poor strength of anti-Stokes signals. The shift in frequency is represented as $\upsilon = \upsilon_s - \upsilon_i$, and it is equivalent to the energy change, since $E = h\upsilon$. The results of Raman spectra are displayed as a function of wavenumber instead of frequency. Wavenumber is defined as $\frac{\text{no. of waves}}{\text{cm}}$. Wavenumber can be calculated by following expression:

$$\text{Wavenumber} = \frac{\text{Frequency}}{c} \tag{1.13}$$

where the value of c is around 2.99×10^8 m s^{-1}, i.e. the speed of light in vacuum. Additionally, wavenumber is inversely proportional to the wavelength since:

$$\text{Frequency} = \frac{c}{\text{Wavelength}} \tag{1.14}$$

To represent wavenumber, mostly cm^{-1} unit is used. The atomic bonds vibrations within the material are responsible for frequency shift in scattering while the phonons energy of material is comparable to the difference of energies between incident and scattered photons. The investigation of scattered frequencies provides important information about the material structure. Generally, materials have a very narrow distribution of bond energies, that is why Raman spectra associated with such materials also show narrow lines. In case of amorphous materials, the bonding energy has a broad distribution that is why Raman spectra associated with amorphous materials have broad signals, which conclude that if Raman spectra have broad signals then material has a disordered structure. In general, RS is a very weak phenomenon. In 10^6–10^8 scattered photons only one Raman scattered photon comes out. This does not make the process unachievable since with high-tech CCD detectors and lasers, very high power densities can be incident to small objects. But it triggers other unacceptable things such as sample degradation and fluorescence. Figure 1.9c shows the fundamental phenomenon, which takes place for one vibration. In that figure, virtual energy states are imaginary states. These states are created by an incident laser light on a sample. Laser sources also determine the energy of mentioned states. In general, most molecules are located at their lowest energy state. The Rayleigh has the greatest intensity among all processes, since a major portion of scattered photons is taken in that way. They do not show any shift in energy. So, this

type of scattering is useless for investigation purposes. Upon illumination by a laser, the electrons present in a vibrational level get excited by a higher vibration level. During the de-excitation process, some electrons return to the initial vibrational energy level. The photons generated during this type of de-excitation have the same wavelength as the incident photons. This is called Raleigh de-excitation or Rayleigh scattering. Some electrons get de-excited to the lower vibrational level with respect to the initial vibrational level. The photons generated in this type of de-excitation have fewer wavelengths than that of incident photons. This process is called anti-stock de-excitation or anti-stock scattering. Rest of the electrons get de-excited to higher vibrational levels with respect to the initial vibrational level. The photons generated in the process have more wavelength than the wavelength of incident photons. This process is Stokes de-excitation or Stokes scattering. Intensity of anti-Stokes scattering also becomes very poor. At higher temperatures, both types of scattering increase. Raman spectroscopy is divided into types according to its way of signal collection, i.e. dispersive Raman spectroscopy and FT-Raman spectroscopy. Both types have their own advantages and can analyze specific samples [167–169].

Finally, having gone through the appropriate theory, all the details of the experimental setup, we are now ready to consider the experimental Raman spectra of CNTs. Raman Spectroscopy provides major information about CNTs structure, defects in CNTs as well as their purity. It is also used in the identification between MWNTs and SWNTs as well as other carbon materials [144]. In general, Raman spectroscopy is more fruitful for SWNTs as compared to MWNTs. For MWNTs, it gives very complex spectra. Because MWNTs behave like a group of SWNTs, the diameter ranges from very small to large [170]. The decoding of the Raman spectra for MWNTs is based on the well-established Raman spectra for SWNTs. It is reported in many articles that Raman spectroscopy has the potential to provide qualitative as well quantitative information about CNTs. An ideal Raman spectra of CNTs have the following important peaks (also see Figure 1.10a):

I. RBM
II. D-Band
III. G-Band
IV. G′-Band

Radial Breathing Mode (RBM) The radial breathing mode (RBM) ($<200\,\mathrm{cm}^{-1}$) is a strong line in the SWNT Raman spectrum. This line is the only strong line that has no analog in the spectra of graphite. It was revealed that it has an elementary dependence on diameter $\omega\mathrm{RBM} = \frac{\alpha\mathrm{RBM}}{dt}$. The RBM is strongly related to a tube diameter. It is inversely proportional to the diameter. For large diameter SWNTs, greater than 2 nm, the RBM may disappear [172]. Due to radial motion of CNT atoms, the RBM is more strongly affected with the environment of a nanotube than the other high-intensity modes. For example, other tubes can be in a bindle or on a supporting substrate. In addition to this fact, the RBM is a direct demonstration of the SWNTs one-dimensional tubular structure that makes it a valuable probe for the properties of nanotubes as well as for the majority of papers concerned

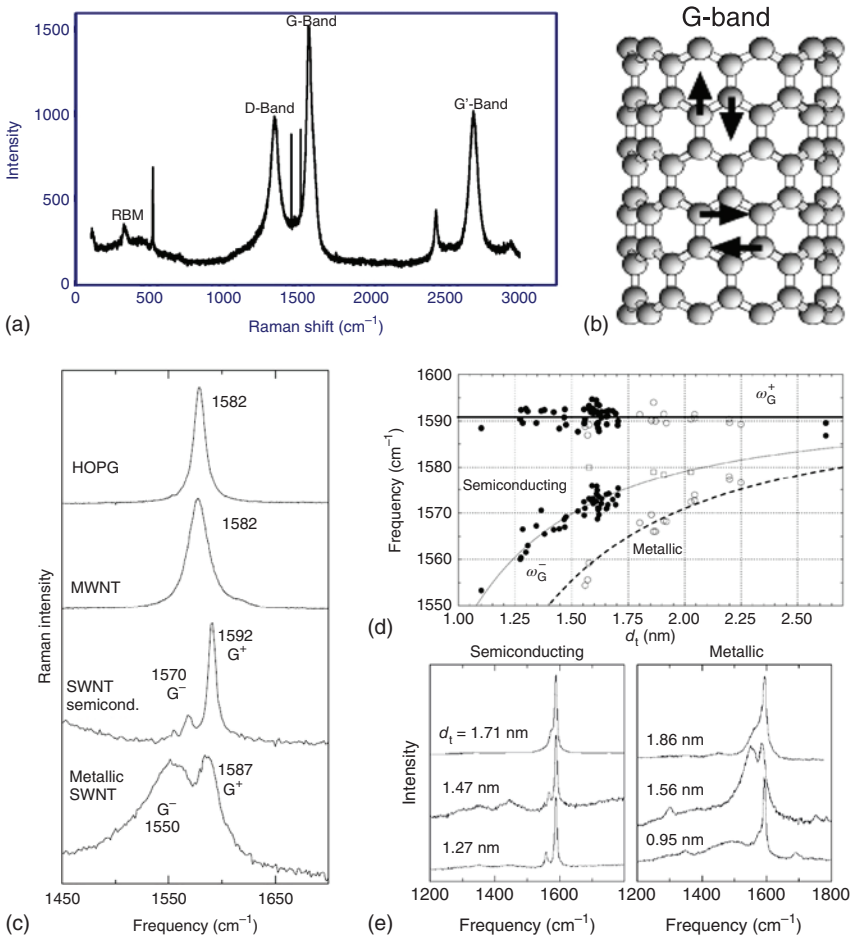

Figure 1.10 Figure (a) shows the Raman spectra of SWNTs. Figure (b) shows the schematic picture of atomic vibrations for the G band modes. Figure (c) represents the G-band peak of various graphitic nanostructures. Figure (d) shows the ω_{G+} and ω_{G-} for different types of SWNTs as a function of the tube diameter. Figure (e) shows the G-band and D-band peaks of Raman spectra of various types of SWNTs. Source: (b, c, e) Jorio et al. [167]/with permission of IOP Publishing and (d) Jorio et al. [171]/with permission of American Physical Society.

with Raman effect in SWNTs. In the case of RBM, peak broadening also has a very meaningful information. The RBM-peak can broaden due to the contribution of different effects. The nanotube sample in a bundle form results in the RBM expansion with regard to the case of an isolated tube, because the interactions between tubes affect ωRBM, and the interactions are determined by the resonant tube position in the bundle. The sample temperature enlarges broadening because of electron–phonon and phonon–phonon interactions [30]. It has been reported that the peaks shift during heating perhaps appears owing to changes in the intra- and inter-tube interactions inside the bundles as well as due to a fewer degree caused by tubes thermal expansion. Therefore, the peaks will expand in case of occurred

temperature differences within the sample (e.g. because of the intensity profile of the impinging beam heating specific areas more than others or due to various couplings to the substrate). Moreover, peaks broadening can be caused by defects in the tubes as well as due to other interactions. Due to the fact that several peaks are narrower than 6 cm^{-1}, it is concluded that broadening caused by electron–phonon interaction is bigger in graphite than in nanotubes [173]. Notably, Raman studies on some samples of nanotubes bundles revealed peaks equal to or greater than 20 cm^{-1} [174]. In addition, low-temperature measurements on free tubes with a big quantity of defects demonstrate line widths up to 0.35 cm^{-1} [171]. Hence, the linewidth is crucially reliant in the nature of sample and in the parameters of measurement.

G-Band In Raman spectra, G-band, a bunch of peaks around 1582 cm^{-1} also verify the existence of CNTs. G-band has the ability to investigate a diameter-dependent study of SWNTs without using RBM. In resonance, for a particular laser light, the metallic character of CNTs is also observed. For CNTs, G-band has six peaks. Out of six, two peaks have maximum intensity and for simplicity, we consider only two peaks, i.e. G+ and G−. These peaks are produced by symmetry breaking of the tangential vibration when the graphene sheet is rolled to make a cylindrically shaped tube. G+ is originated through atomic displacements along the tube axis and G− is produced by atomic displacement along the circumferential direction (see Figure 1.10b,c). Figure 1.10c shows the line shape difference of G− for semiconducting and MWCNTs and it is broaden for metallic with respect to semiconducting CNTs (see Figure 1.10c), and its broadening is coming from free electrons in nanotubes with metallic behavior [175–177]. If charged impurity exists in SWNTs then G-band for semiconducting CNTs shows the behavior of metallic CNTs [178]. If talking about a diameter-dependent study of G− band then the frequency of G+ does affected by diameter but in the frequency of G− band shifting with variation in diameter of CNTs is observed (see Figure 1.10d,e) [179, 180]. Hence, G-band and its splitting may be used for the CNTs diameter calculation. Recently, some research groups gave the evidence about G-band formation from double resonance mechanisms [176–181]. In that case, the intensity of the G-band very much depends on CNTs defects, and the frequency of G-band depends on the laser energy. This evidence creates complications in the use of Raman spectroscopy for SWNTs. However, it can be observed that double, as well as single resonance, show the same intensity for a defective material. For defect-less materials, intensity of single resonance is double as compared to double resonance phenomenon [182, 183]. So, according to this report, Raman spectroscopy is the only effective for good quality of SWNTs.

Disorder Bands (D-Band and G′-Band) A bunch of peaks appear in Raman spectra of CNTs around 1332 and 2700 cm^{-1}. It represents defects and disorders in the structure of CNTs. It is highlighted in both types of CNTs. Due to double resonance criteria, D-band also appears due to some specific chirality [184]. In case of isolated SWNTs, D-band is split into two parts. Split distance of D-band relates to energy of incident light. G′-Band shows an intrinsic property of graphite. The G′-Band is caused by

two-phonon scattering around the K-point of the Brillouin-zone. $G^{|}$-mode comes in a picture only at high-defect density; it has less significant as compared to the first order mode. The mode has more contributions from regions near the K and M-points, $G^{|}$ peak is visualized in Raman spectra at 2700 and 2730 cm^{-1}. It has been reported that $G^{|}$ peak provides information about CNTs where other phonon modes failed and the metallicity of CNTs is responsible for the intensity of $G^{|}$ peak [185].

1.3 Conclusion

CNT is one of the most rigorously researched materials in the contemporary world. Owing to their extraordinary properties, CNTs have become one of the front runners in the world of contemporary research. If a cross-section area of CNTs walls is considered then the values of elastic modulus and tensile strength have been estimated as 1 TPa and 100 GPa, respectively. The mechanical strength of CNTs has been found 10 times more as compared to any other fiber. Generally, MWNTs show metallic behavior with a very high current capacity ($\sim 10^9$ A cm^{-2}). Individual walls in MWNTs can act as metallic or semiconducting as per folding angle of graphene sheet from which CNT is constructed. The orientation of graphene sheet with the tube axis is defined as chirality. Room-temperature thermal conductivity of SWNTs can even reach up to 3500 W m^{-1} K^{-1} that is more than of a diamond. Because of these ultimate properties, CNTs are being used in a variety of nanosensors, biosensors, optoelectronic devices such as photodetectors, solar cells, and light-emitting diodes, in different types of high-performance electronic devices, as reinforcement in different composite systems, etc. For the preparation of devices at nanoscale, where we deal with the ultra-small regime, control of synthesis and growth of CNTs having precise specifications is very important. Having understood the importance of CNTs, we made a detailed discussion on the various allotropes of carbon, especially on CNTs. The basic structures of CNTs, defects in structure, electronics, optoelectronics, and chemical as well as mechanical properties of CNTs have been covered. A detailed discussion on the various synthesis techniques of CNTs with comparative analysis have been covered. CVD method is the most widely used method to grow MWNTs and SWNTs. There are different factors such as dynamics of hydrocarbons as well as carrier gases, growth temperature, temperature ramp, catalyst engineering, substrate engineering, etc. that affect the specifications of CNTs. We made a detailed study on all mentioned factors. For CNTs analysis, various nanomaterials characterization tools such as SEM, TEM, AFM, Raman Spectroscopy, XRD, etc. are required. A detailed study on mentioned characterization tools, their instrumentation, and utilization for CNTs has been made. The chapter will be helpful for the development of modern electron materials and applications.

Declaration of Competing Interest

Authors do not have any conflict of interest.

Companies Dealing with Chemically Modified CNTs

I. Sigma-Aldrich, USA
II. Cheaptubes.com
III. Nanoshel, UK
IV. Nanostructured & Amorphous Materials, Inc., USA

Acknowledgments

This work was supported by Russian Science Foundation (Grant No. 21-79-00272).

References

1 Tripathi, N. and Islam, S.S. (2017). A new approach for orientation controlled growth of CNTs: an in-depth analysis on the role of oxygen plasma treatment to catalyst. *Appl. Nanosci.* 7: 125–129.
2 Tripathi, N., Mishra, P., Joshi, B. et al. (2014). Catalyst free, excellent quality and narrow diameter of CNT growth on Al_2O_3 by thermal CVD technique. *Phys. E* 62: 43–47.
3 Sharma, P., Pavelyev, V., Kumar, S. et al. (2020). Analysis on the synthesis of vertically aligned carbon nanotubes: growth mechanism and techniques. *J. Mater. Sci.: Mater. Electron.* 31: 4399–4443.
4 Kumar, M. and Ando, Y. (2010). Chemical vapor deposition of carbon nanotubes: a review on growth mechanism and mass production. *J. Nanosci. Nanotechnol.* 10: 3739–3758.
5 Tripathi, N., Mishra, P., Joshi, B., and Islam, S.S. (2015). Precise control over physical characteristics of carbon nanotubes by differential variation of argon flow rate during chemical vapor deposition processing: a systematic study on growth kinetics. *Mater. Sci. Semicond. Process.* 35: 207–215.
6 Krueger, A. (2010). *Carbon Materials and Nanotechnology*. Weinheim: Wiley-VCH Verlag GmbH & Co. KGaA.
7 Meyyappan, M. (2004). *Carbon Nanotubes Science and Applications*. NASA, Ames Research Center Moffett Field, CA, CRC Press.
8 Debye, P. and Scherrer, P. (1917). Interferenzen a regellos orientierten teilchen im Röntgenlicht. *Phys. Z* 18: 291.
9 Geim, A.K. and Novoselov, K.S. (2007). The rise of graphene. *Nat. Mater.* 6: 183.
10 Bokros, J.C. (1969). *Chemistry and Physics of Carbon*, vol. 5 (ed. P.L. Walker Jr.). New York: Marcel Dekker Inc.
11 Pierson, H.O. (1993). *Handbook of Carbon, Graphite, Diamond and Fullerenes, Properties, Processing and Applications*. Park Ridge, NJ: Noyes Publications.
12 Guy, G. (1959). *Elements of Physical Metallurgy*. Reading, MA: Addison-Wesley Publishing.

13 Cullity, D. (1956). *Elements of X-ray Diffraction*. Reading, MA: Addison-Wesley Publishing.

14 Spear, K.E. (1969). Diamond: ceramic coating of the future. *J. Am. Ceram. Soc.* 72: 171–191.

15 Eggers, D.F. Jr. and Halsey, G.D. Jr. (1964). *Physical Chemistry*. New York: Wiley.

16 Gardinier, F. (1988). Physical properties of superabrasives. *Ceram. Bull.* 67: 1006.

17 Spear, K.E., Phelps, A.W., and White, W.B. (1990). Diamond polytypes and their vibrational spectra. *J. Mater. Res.* 5: 2271.

18 Dawson, J.B. (1967). *The Properties of Diamond* (ed. J.E. Field), 539–554. London: Academic Press.

19 Wong, H.S.P. and Jiakinwande, D.E. (2001). *Carbon Nanotube and Graphene Device Physics*. Cambridge University Press.

20 Pauling, L. (1960). *The Nature of Chemical Bonds*. Cornell University Press.

21 Bhushan, B. (2011). *Nanoscience and Technology (Scanning Probe Microscopy in Nanoscience and Nano Technology)*. Springer.

22 Rogers, G.L. (1950). Gabor diffraction microscopy: the hologram as a generalized zone-plate. *Nature* 166: 237.

23 Radushkevich, L.V. and Lukyanovich, V.M. (1952). O struktureugleroda, obrazujucegosjapritermiceskomrazlozeniiokisiuglerodanazeleznomkontakte. *Zurn. Fisic. Chim.* 26: 88.

24 Baker, R.J., Mengden, G.A., and Bull, J.J. (1972). Karyotypic studies of thirty-eight species of North American snakes. *Copeia* 1972: 257.

25 Oberlin, A., Endo, M., and Koyama, T. (1976). Filamentous growth of carbon through benzene decomposition. *J. Cryst. Growth* 32: 3.

26 Dupuis (2005). The catalyst in the CCVD of carbon nanotubes- a review. *Prog. Mater. Sci.* 50 (8): 929–961.

27 Aqel, A., Abou El-Nour, K.M.M., Ammar, R.A.A., and Al-Warthan, A. (2012). Carbon nanotubes, science and technology part (I) structure, synthesis and characterization. *Arabian J. Chem.* 5: 1–23.

28 Saito, R., Dresselhaus, G., and Dresselhaus, M.S. (1998). *Physical Properties of Carbon Nanotubes*. Imperial College Press.

29 McEuen, P.L. (1999). Disorder, pseudospins, and backscattering in carbon nanotubes. *Phys. Rev. Lett.* 24: 5098.

30 Dresselhaus, M.S.E. (2000). Phonons in carbon nanotubes. *Adv. Phys.* 49: 705.

31 Hone, J. (2000). Quantized phonon spectrum of single-wall carbon nanotubes. *Science* 289: 1730.

32 Tans, S.J. (1997). Individual single-wall carbon nanotubes as quantum wires. *Nature* 386: 474.

33 Frank, S. (1998). Carbon nanotube quantum resistors. *Science* 280: 1744.

34 Soh, H.T. (1999). Integrated nanotube circuits: controlled growth and ohmic contacting of single-walled carbon nanotubes. *Appl. Phys. Lett.* 75: 627.

35 Rao, A.M. (1997). Diameter-selective Raman scattering from vibrational modes in carbon nanotubes. *Science* 275: 187.

36 Bachilo, S.M. (2002). Structure-assigned optical spectra of single-walled carbon nanotubes. *Science* 298: 2361.

37 Hagen, A. and Hertel, T. (2003). Quantitative analysis of optical spectra from individual single-wall carbon nanotubes. *Nano Lett.* 3: 383.

38 Paulson, S. (1999). In situ resistance measurements of strained carbon nanotubes. *Appl. Phys. Lett.* 75: 2936.

39 Tsang, S.C. (1994). A simple chemical method of opening and filling carbon nanotubes. *Nature* 372: 159.

40 Ajayan, P.M. (1995). Carbon nanotubes as removable templates for metal-oxide nanocomposites and nanostructures. *Nature* 375: 564.

41 Dujardin, E. (1994). Capillarity and wetting of carbon nanotubes. *Science* 265: 1850.

42 Ugarte, D. (1996). Nanocapillarity and chemistry in carbon nanotubes. *Science* 274: 1897.

43 Zhao, J., Lu, J.P., Han, J., and Yang, C. (2003). Noncovalent functionalization of carbon nanotubes by aromatic organic molecules. *Appl. Phys. Lett.* 82: 3746.

44 Kruger, M. (2003). Sensitivity of single multiwalled carbon nanotubes to the environment. *New J. Phys.* 5: 138.

45 Zhao, J., Buldum, A., and Han, J. (2000). First-principles study of Li-intercalated carbon nanotube ropes. *Phys. Rev. Lett.* 85: 1706.

46 Frackowiak, E., Gautier, S., Gaucher, H. et al. (1999). Electrochemical storage of lithium in multiwalled carbon nanotubes. *Carbon* 37: 61.

47 Wu, G.T. (1999). Structure and lithium insertion properties of carbon nanotubes. *J. Electrochem. Soc.* 146: 1696.

48 Lehman, J.H., Terrones, M., Mansfield, E. et al. (2011). Evaluating the characteristics of multiwall carbon nanotubes. *Carbon* 4 (9): 2581.

49 Bao, B. (1999). Carbon nanotubes science and application. *Chem. Phys. Lett.* 307: 153.

50 Bonard, J.M., Croci, M., Klinke, C. et al. (2002). Carbon nanotube films as electron field emitters. *Carbon* 40: 1715.

51 Thrower, P.A. (1969). The study of defects in graphite by transmission electron spectroscopy. *Chem. Phys. Carbon* 5: 217.

52 Terrones, M., Terrones, G., and Terrones, H. (2002). Structure, chirality, and formation of giant icosahedral fullerenes and spherical graphitic onions. *Struct. Chem.* 13: 373.

53 Charlier, J.C., Terrones, M., Baxendale, M. et al. (2002). Enhanced electron field emission in B-doped carbon nanotubes. *Nano Lett.* 2: 1191–1195.

54 Girit, C.O., Meyer, J.C., Erni, R. et al. (2009). Graphene at the edge: stability and dynamics. *Science* 323: 1705.

55 Terrones, M., Jorio, A., Endo, M. et al. (2004). New direction in nanotube science. *Mater. Today* 7: 30.

56 Maciel, O., Delgado, J.C., Silva, E.C. et al. (2009). Synthesis, electronic structure, and Raman scattering of phosphorus-doped single-wall carbon nanotubes. *Nano Lett.* 9: 2267.

57 Maciel, O., Anderson, N., Pimenta, M.A. et al. (2008). Electron and phonon renormalization near charged defects in carbon nanotubes. *Nat. Mater.* 7: 878.

58 Sadegh, H. and Shahryari-ghoshekandi, R. (2015). Functionalization of carbon nanotubes and its application in nanomedicine: a review. *Nanomed. J.* 2: 231–248.

59 Mallakpour, S. and Soltanian, S. (2016). Surface functionalization of carbon nanotubes: fabrication and applications. *RSC Adv.* 6: 109916–109935.

60 Venkatesh, K., Arthanareeswaran, G., Chandra Bose, A. et al. (2021). Diethylenetriaminepentaacetic acid-functionalized multi-walled carbon nanotubes/titanium oxide-PVDF nanofiber membrane for effective separation of oil/water emulsion. *Sep. Purif. Technol.* 257: 117926.

61 Bouanis, F.Z., Bensifia, M., Florea, I. et al. (2021). Non-covalent functionalization of single walled carbon nanotubes with Fe-/Co-porphyrin and Co-phthalocyanine for field-effect transistor applications. *Org. Electron.* 96: 106212.

62 He, X., Kevlishvili, I., Murcek, K. et al. (2021). Photocycloaddition of enones to single-walled carbon nanotubes creates fluorescent quantum defects. *ACS Nano* 15: 4833–4844.

63 Khan, D., Ali, Z., Asif, D. et al. (2021). Incorporation of carbon nanotubes in photoactive layer of organic solar cells. *Ain Shams Eng. J.* 12: 897–900.

64 Muhammad-Ahson Aslam, M., Kuo, H.-W., Den, W. et al. (2021). Functionalized carbon nanotubes (CNTs) for water and wastewater treatment: preparation to application. *Sustainability* 13: 5717.

65 Ma, P.C., Siddiqui, N.A., Marom, G., and Kim, J.K. (2010). Dispersion and functionalization of carbon nanotubes for polymer-based nanocomposites: a review. *Composites, Part A* 41: 1345–1367.

66 Hirsch, A. (2002). Functionalization of single-walled carbon nanotubes. *Angew. Chem. Int. Ed.* 41: 1853–1859.

67 Hirsch, A. and Vostrowsky, O. (2005). Functionalization of carbon nanotubes. *Top. Curr. Chem.* 245: 193–237.

68 Kim, W., Nair, N., Lee, C.Y., and Strano, M.S. (2008). Covalent functionalization of singlewalled carbon nanotubes alters their densities allowing electronic and other types of separation. *J. Phys. Chem. C* 112: 7326–7331.

69 Niyogi, S., Hamon, M.A., Hu, H. et al. (2002). Chemistry of single-walled carbon nanotubes. *Acc. Chem. Res.* 35: 1105–1113.

70 Tasis, D., Tagmatarchis, N., Georgakilas, V., and Prato, M. (2003). Soluble carbon nanotubes. *Chem. Eur. J.* 9: 4000–4008.

71 Sinnott, S.B. (2002). Chemical functionalization of carbon nanotubes. *J. Nanosci. Nanotechnol.* 2: 113–123.

72 Mickelson, E.T., Huffman, C.B., Rinzler, A.G. et al. (1998). Fluorination of single-wall carbon nanotubes. *Chem. Phys. Lett.* 296: 188–194.

73 Kelly, K.F., Chiang, I.W., Mickelson, E.T. et al. (1993). Insight into the mechanism of sidewall functionalization of single-walled nanotubes: an STM study. *Chem. Phys. Lett.* 313: 445–450.

74 Touhara, H., Inahara, J., Mizuno, T. et al. (2002). Fluorination of cup-stacked carbon nanotubes, structure and properties. *Fluorine Chem.* 114: 181–188.

75 Stevens, J.L., Huang, A.Y., Peng, H. et al. (2003). Sidewall amino-functionalization of SWNTs through fluorination and subsequent reactions with terminal diamines. *Nano Lett.* 3: 331–336.

76 Tseng, C.-H., Wang, C.-C., and Chen, C.-Y. (2007). Functionalizing carbon nanotubes by plasma modification for the preparation of covalent-integrated epoxy composites. *Chem. Mater.* 19: 308–315.

77 Xie, L., Xu, F., Qiu, F. et al. (2007). Single-walled carbon nanotubes functionalized with high bonding density of polymer layers and enhanced mechanical properties of composites. *Macromolecules* 40: 3296–3305.

78 Shi, X., Wang, J., Jiang, B., and Yang, Y. (2013). Hindered phenol grafted carbon nanotubes for enhanced thermal oxidative stability of polyethylene. *Polymer* 54: 1167–1176.

79 Zhou, Z., Yan, X., Cook, T.R. et al. (2016). Engineering functionalization in a supramolecular polymer: hierarchical self-organization of triply orthogonal non-covalent interactions on a supramolecular coordination complex platform. *J. Am. Chem. Soc.* 138: 806–809.

80 Ji, X., Xu, Y., Zhang, W. et al. (2016). Review of functionalization, structure and properties of graphene/polymer composite fibers. *Composites, Part A* 87: 29–45.

81 Orellana, W. and Correa, J.D. (2015). Noncovalent functionalization of carbon nanotubes and graphene with tetraphenylporphyrins: stability and optical properties from ab initio calculations. *J. Mater. Sci.* 50: 898–905.

82 McCarthy, B., Coleman, J.N., Czerw, R. et al. (2001). Microscopy studies of nanotube-conjugated polymer interactions. *Synth. Met.* 121: 1225–1226.

83 Gong, X., Liu, J., Baskaran, S. et al. (2000). Surfactant-assisted processing of carbon nanotube/polymer composites. *Chem. Mater.* 12: 1049–1052.

84 Vaisman, L., Marom, G., and Wagner, H.D. (2006). Dispersions of surface-modified carbon nanotubes in water-soluble and water-insoluble polymers. *Adv. Funct. Mater.* 16: 357–363.

85 Geng, Y., Liu, M.Y., Li, J. et al. (2008). Effects of surfactant treatment on mechanical and electrical properties of CNT/epoxy nanocomposites. *Composites, Part A* 39: 1876–1883.

86 Islam, M.F., Rojas, E., Bergey, D.M. et al. (2003). High weight fraction surfactant solubilization of single-wall carbon nanotubes in water. *Nano Lett.* 3: 269–273.

87 Yu, J., Grossiord, N., Koning, C.E., and Loos, J. (2007). Controlling the dispersion of multi-wall carbon nanotubes, in aqueous surfactant solution. *Carbon* 45: 618–623.

88 Whitsitt, E.A. and Barron, A.R. (2003). Silica coated single walled carbon nanotubes. *Nano Lett.* 3: 775–778.

89 Vaisman, L., Wagner, H.D., and Marom, G. (2006). The role of surfactants in dispersion of carbon nanotubes. *Adv. Colloid Interface Sci.* 128–130: 37–46.

90 Yuan, W. and Chan-Park, M.B. (2012). Covalent cum noncovalent functionalizations of carbon nanotubes for effective reinforcement of a solution cast composite film. *ACS Appl. Mater. Interfaces* 4: 2065–2073.

91 Yola, M.L. and Atar, N. (2021). Novel voltammetric tumor necrosis factor-alpha (TNF-α) immunosensor based on gold nanoparticles involved in thiol-functionalized multi-walled carbon nanotubes and bimetallic Ni/Cu-MOFs. *Anal. Bioanal.Chem.* 413: 2481–2492.

92 Wang, S., Wang, M., Li, C. et al. (2020). A highly sensitive and stable electrochemiluminescence immunosensor for alpha-fetoprotein detection based on luminol-AgNPs@Co/Ni-MOF nanosheet microflowers. *Sens. Actuators, B* 311: 127919.

93 Pouya, Z.A., Tofighy, M.A., and Mohammadi, T. (2021). Synthesis and characterization of polytetrafluoroethylene/oleic acid-functionalized carbon nanotubes composite membrane for desalination by vacuum membrane distillation. *Desalination* 503: 114931.

94 González-Muñoz, D., Martín-Somer, A., Strobl, K. et al. (2021). Enhancing visible-light photocatalysis via endohedral functionalization of single-walled carbon nanotubes with organic dyes. *ACS Appl. Mater. Interfaces* 13: 24877–24886.

95 Choi, E.Y., Kim, M.H., Lee, S.Y. et al. (2021). Reactivity estimation of polybutylene terephthalate with noncovalently functionalized multiwalled carbon nanotubes and reactivity effect on the composite reinforcement. *Compos. Sci. Technol.* 201: 108549.

96 Zhao, Y.L., Hu, L., Grüner, G., and Stoddart, J.F. (2008). A tunable photosensor. *J. Am. Chem. Soc.* 130.

97 Barone, P.W., Baik, S., Heller, D.A., and Strano, M.S. (2005). Near-infrared optical sensors based on single-walled carbon nanotubes. *Nat. Mater.* 4: 86–92.

98 Li, X., Jia, Y., Wei, J. et al. (2010). Solar cells and light sensors based on nanoparticle-grafted carbon nanotube films. *ACS Nano* 4: 2142–2148.

99 Liu, S., Ye, J., Cao, Y. et al. (2009). Tunable hybrid photodetectors with superhigh responsivity. *Small* 5: 2371–2376.

100 Bekyarova, E., Davis, M., Burch, T. et al. (2004). Chemically functionalized single-walled carbon nanotubes as ammonia sensors. *J. Phys. Chem. B* 108: 19717–19720.

101 Sin, M.L.Y., Chow, G.C.T., Wong, G.M.K. et al. (2007). Ultralow-power alcohol vapor sensors using chemically functionalized multiwalled carbon nanotubes. *IEEE Trans. Nanotechnol.* 6: 571–577.

102 Niu, L., Luo, Y., and Li, Z. (2007). A highly selective chemical gas sensor based on functionalization of multi-walled carbon nanotubes with poly(ethylene glycol). *Sens. Actuators, B* 126: 361–367.

103 Dhall, S., Jaggi, N., and Nathawat, R. (2013). Functionalized multiwalled carbon nanotubes based hydrogen gas sensor. *Sens. Actuators, A* 201: 321–327.

104 Kong, J., Chapline, M.G., and Dai, H. (2001). Functionalized carbon nanotubes for molecular hydrogen sensors. *Adv. Mater.* 13: 1384–1386.

105 Sayago, I., Terrado, E., Lafuente, E. et al. (2005). Hydrogen sensors based on carbon nanotubes thin films. *Synth. Met.* 148: 15–19.
106 Iijima, S., Ichihashi, T., and Ando, Y. (1992). Pentagons, heptagons and negative curvature in graphite microtubule growth. *Nature* 356: 776.
107 Ryu, J.H., Kang, J.S., and Park, K.C. (2012). Carbon nanotube electron emitter for X-ray imaging. *Materials* 5: 2353.
108 Jensen, K., Weldon, J., Garcia, H., and Zettl, A. (2007). Nanotube radio. *Nano Lett.* 11: 3508.
109 Rueckes, T., Kim, K., Joselevich, E. et al. (2000). Carbon nanotube-based nonvolatile random access memory for molecular computing. *Science* 289: 5476.
110 Xi, N. and La, K. (2012). *Nano Optoelectronic Sensors and Devices: Nanophotonics from Design to Manufacturing*. Elsevier.
111 Yamashita, S., Saito, Y., and Choi, J.H. (2013). *Carbon Nanotubes and Graphene for Photonic Applications*. Woodhead Publishing.
112 Melisi, D., Nitti, M.A., Valentini, M. et al. (2014). Photodetectors based on carbon nanotubes deposited by using a spray technique on semi-insulating gallium arsenide. *J. Nanotechnol.* 5: 1999.
113 Sazonova, V., Yaish, Y., Üstünel, H. et al. (2004). A tunable carbon nanotube electromechanical oscillator. *Nature* 431: 284.
114 Fennimore, M., Yuzvinsky, T.D., Han, W.-Q. et al. (2003). Rotational actuators based on carbon nanotubes. *Nature* 424: 408.
115 Kim, P. and Lieber, C.M. (1999). Nanotube nanotweezers. *Science* 286: 2148.
116 Zhang, Q. (2012). *Carbon Nanotubes and Their Applications*, Pan Stanford Series on Carbon Based Nanomaterials, vol. 1. CRC Press.
117 Popov, A.M., Lebedeva, I.V., Knizhnik, A.A. et al. (2014). Force and magnetic field sensor based on measurement of tunnelling conductance between ends of coaxial carbon nanotubes. *Comput. Mater. Sci.* 92: 84.
118 Poot, M. and van der Zant, H.S.J. (2012). Mechanical systems in the quantum regime. *Phys. Rep.* 511: 273.
119 Saito, Y., Yoshikawa, T., Inagaki, M. et al. (1993). Growth and structure of graphitic tubules and polyhedral particles in arc-discharge. *Chem. Phys. Lett.* 204: 227.
120 Iijima, S. (1991). Helical microtubules of graphitic carbon. *Nature* 354 (6348): 56.
121 Journet, C., Maser, W.K., Bernier, P. et al. (1997). Large-scale production of single-walled carbon nanotubes by the electric-arc technique. *Nature* 388: 756.
122 Saito, Y., Nishikubo, K., Kawabata, K., and Matsumoto, T. (1996). Carbon nanocapsules and single-layered nanotubes produced with platinum-group metals (Ru, Rh, Pd, Os, Ir, Pt) by arc discharge. *J. Appl. Phys.* 80: 3062.
123 Farhat, S., de La Chapelle, M.L., Loiseau, A. et al. (2001). Diameter control of single-walled carbon nanotubes using argon–helium mixture gases. *J. Chem. Phys.* 115: 6752.
124 Tang, D., Xie, S., Liu, W. et al. (2000). Evidence for an open-ended nanotube growth model in arc discharge. *Carbon* 38: 480.

125 Ebbesen, T. and Ajayan, P. (1992). Large-scale synthesis of carbon nanotubes. *Nature* 358: 220.

126 Cadek, M., Murphy, R., McCarthy, B. et al. (2002). Optimisation of the arc-discharge production of multi-walled carbon nanotubes. *Carbon* 40: 923.

127 Journet, C. and Bernier, P. (1998). Production of carbon nanotubes. *Appl. Phys. A* 67: 1.

128 Bolshakov, A.P., Uglov, S., Saveliev, A. et al. (2002). A novel CW laser–powder method of carbon single-wall nanotubes production. *Diamond Relat. Mater.* 11: 927.

129 Kokai, F., Takahashi, K., Yudasaka, M. et al. (1999). Growth dynamics of single-wall carbon nanotubes synthesized by CO_2 laser vaporization. *J. Phys. Chem.* B103: 4346.

130 Wei, B.Q., Vajtai, R., Jung, Y. et al. (2002). Microfabrication technology: organized assembly of carbon nanotubes. *Nature* 416: 495.

131 Sengupta, J. (2018). Carbon nanotube fabrication at industrial scale: opportunities and challenges, Chapter 9. In: *Handbook of Nanomaterials for Industrial Applications* (ed. C.M. Hussain), 172–194. Elsevier.

132 Nihei, M., Kawabata, A., Kondo, D. et al. (2005). Electrical properties of carbon nanotube bundles for future via interconnects. *Jpn. J. Appl. Phys.* 44: 1626.

133 Dikonimos Makris, T., Giorgi, L., Giorgi, R. et al. (2005). CNT growth on alumina supported nickel catalyst by thermal CVD. *Diamond Relat. Mater.* 14: 815.

134 Wu, Y. and Yang, P. (2001). Direct observation of vapor–liquid–solid nanowire growth. *J. Am. Chem. Soc.* 123: 3165–3166.

135 Tripathi, N., Mishra, P., Harsh, H., and Islam, S.S. (2015). Fine-tuning control on CNT diameter distribution, length and density using thermal CVD growth at atmospheric pressure: an in-depth analysis on the role of flow rate and flow duration of acetylene (C_2H_2) gas. *Appl. Nanosci.* 5: 19.

136 Shaikjee, A. and Coville, N.J. (2012). The role of the hydrocarbon source on the growth of carbon materials. *Carbon* 50: 3376–3398.

137 Hernadi, K., Fonseca, A., Nagy, J.B. et al. (1996). Fe-catalyzed carbon nanotube formation. *Carbon* 34: 1249.

138 Kong, J., Cassell, A.M., and Dai, H. (1998). Chemical vapor deposition of methane for single-walled carbon nanotubes. *Chem. Phys. Lett.* 292: 567.

139 Fan, S., Chapline, M., Frankline, N. et al. (1999). Self-oriented regular arrays of carbon nanotubes and their field emission properties. *Science* 283: 512.

140 Sen, R., Govindaraj, A., and Rao, C.N.R. (1997). Carbon nanotubes by the metallocene route. *Chem. Phys. Lett.* 267: 276.

141 Nikolaev, P., Bronikowski, M.J., Bradley, R.K. et al. (1999). Gas-phase catalytic growth of single-walled carbon nanotubes from carbon monoxide. *Chem. Phys. Lett.* 313: 91.

142 Endo, M., Fijiwara, H., and Fukunaga, E. (1991). *18th Meeting Japanese, Carbon Society*, 34. Saitama: Japanese Carbon Society.

143 Endo, M., Takeuchi, K., Igarashi, S. et al. (1993). The production and structure of pyrolytic carbon nanotubes (PCNTs). *J. Phys. Chem. Solids* 54: 1841.

144 Jose-Yacaman, M., Miki-Yoshida, M., Rendon, L., and Santiesteban, J.G. (1993). Catalytic growth of carbon microtubules with fullerene structure. *Appl. Phys. Lett.* 62: 657.

145 Liua, Z., Cheb, R., Xu, Z., and Peng, L. (2002). Preparation of Fe-filled carbon nanotubes by catalytic decomposition of cyclohexane. *Synth. Met.* 128: 191.

146 Li, N., Chen, X., Stoica, L. et al. (2007). The catalytic synthesis of three-dimensional hierarchical carbon nanotube composites with high electrical conductivity based on electrochemical iron deposition. *Adv. Mater.* 19: 2957.

147 Morjan, R.E., Nerushev, O.A., Sveningsson, M. et al. (2004). Growth of carbon nanotubes from C_{60}. *Appl. Phys. A* 78: 253.

148 Dai, H., Rinzler, A.G., Nikolaev, P. et al. (1996). Single-wall nanotubes produced by metal-catalyzed disproportionation of carbon monoxide. *Chem. Phys. Lett.* 260: 471.

149 Satishkumar, B.C., Govindaraj, A., Sen, R., and Rao, C.N.R. (1998). Single-walled nanotubes by the pyrolysis of acetylene-organometallic mixtures. *Chem. Phys. Lett.* 293: 47.

150 Flahaut, E., Govindaraj, A., Peigney, A. et al. (1999). Synthesis of single-walled carbon nanotubes using binary (Fe, Co, Ni) alloy nanoparticles prepared in situ by the reduction of oxide solid solutions. *Chem. Phys. Lett.* 300: 236.

151 Cheng, H.M., Li, F., Sun, X. et al. (1998). Bulk morphology and diameter distribution of single-walled carbon nanotubes synthesized by catalytic decomposition of hydrocarbons. *Chem. Phys. Lett.* 289: 602.

152 Maruyama, S., Kojima, R., Miyauchi, Y. et al. (2002). Low-temperature synthesis of high-purity single-walled carbon nanotubes from alcohol. *Chem. Phys. Lett.* 360: 229.

153 Okubo, S., Sekine, T., Suzuki, S. et al. (2004). Purification of single-wall carbon nanotubes synthesized from alcohol by catalytic chemical vapor deposition. *Jpn. J. Appl. Phys.* 43: L396.

154 Nasibulin, G., Moisala, A., Jiang, H., and Kauppinen, E.I. (2006). High quality double wall carbon nanotubes with a defined diameter distribution by chemical vapor deposition from alcohol. *J. Nanopart. Res.* 8: 465.

155 Murakami, Y., Miyauchi, Y., Chiashi, S., and Maruyama, S. (2003). Direct synthesis of high-quality singlewalled carbon nanotubes on silicon and quartz substrates. *Chem. Phys. Lett.* 377: 49.

156 Murakami, Y., Chiashi, S., Miyauchi, Y. et al. (2004). Growth of vertically aligned single-walled carbon nanotube films on quartz substrates and their optical anisotropy. *Chem. Phys. Lett.* 385: 298.

157 Xiang, R., Einarsson, E., Okawa, J. et al. (2009). Acetylene-accelerated alcohol catalytic chemical vapor deposition growth of vertically aligned single-walled carbon nanotubes. *J. Phys. Chem. C* 113: 7511.

158 Hata, K., Futaba, D.N., Mizuno, K. et al. (2004). Water-assisted highly efficient synthesis of impurity-free single-walled carbon nanotubes. *Science* 306: 1362.

159 Zhong, G., Hofmann, S., Yan, F. et al. (2009). Acetylene: a key growth precursor for single-walled carbon nanotube forests. *J. Phys. Chem. C* 113: 17321.

160 Ding, F., Larsson, P., Larsson, J.A. et al. (2008). The importance of strong carbon-metal adhesion for catalytic nucleation of single-walled carbon nanotubes. *Nano Lett.* 8: 463.

161 Moisala, A., Nasibulin, A.G., and Kauppinen, E.I. (2003). The role of metal nanoparticles in the catalytic production of single-walled carbon nanotubes—a review. *J. Phys. Condens. Mater.* 15: S3011.

162 Ago, H., Komatsu, T., Ohshima, S. et al. (2000). Dispersion of metal nanoparticles for aligned carbon nanotube arrays. *Appl. Phys. Lett.* 77: 79.

163 Tripathi, N., Pavelyev, V., and Islam, S.S. (2017). Synthesis of carbon nanotubes using green plant extract as catalyst: unconventional concept and its realization. *Appl. Nanosci.* 7: 557–566.

164 Domagała, K., Borlaf, M., Traber, J. et al. (2019). Purification and functionalisation of multi-walled carbon nanotubes. *Mater. Lett.* 253: 272–275.

165 Biro, L.P., Khanh, N.Q., Vertesy, Z. et al. (2002). Catalyst traces and other impurities in chemically purified carbon nanotubes grown by CVD. *Mater. Sci. Eng., C* 19: 9–13.

166 Tripathi, N., Pavelyev, V., and Islam, S.S. (2018). Tunable growth of single-wall CNTs by monitoring temperature increasing rate. International. *Nano Lett.* 8: 1–9.

167 Jorio, A., Pimenta, M.A., Filho, A.G.S. et al. (2003). Characterizing carbon nanotube samples with resonance Raman scattering. *New J. Phys.* 5: 139.

168 Jorio, A., Saito, R., Dresselhaus, G., and Dresselhaus, M.S. (2011). *Raman Spectroscopy in Graphene Related Systems*. Wiley-VCH.

169 Zumbusch, A., Holtom, G.R., and Xie, X.S. (1999). Three-dimensional vibrational imaging by coherent anti-Stokes Raman scattering. *Phys. Rev. Lett.* 82: 4142.

170 Tan, H., Hu, C.Y., Dong, J. et al. (2001). Polarization properties, high-order Raman spectra, and frequency asymmetry between Stokes and anti-Stokes scattering of Raman modes in a graphite whisker. *Phys. Rev. B* 64: 214301.

171 Jorio, A., Filho, A.G.S., Dresselhaus, G. et al. (2002). G-band resonant Raman study of 62 isolated single-wall carbon nanotubes. *Phys. Rev. B* 65: 155412.

172 Lina, D.H.M., Manaraa, D., Reis, P.L. et al. (2014). The use of different dispersive Raman spectrometers for the analysis of uranium compounds. *Vib. Spectrosc.* 73: 102.

173 Raravikar, R., Keblinski, P., Rao, A.M. et al. (2002). Temperature dependence of radial breathing mode Raman frequency of single-walled carbon nanotubes. *Phys. Rev. B* 66: 235424.

174 Bandow, S., Asaka, S., Saito, Y. et al. (1998). Effect of growth temperature on the diameter distribution and chirality of single-wall carbon nanotubes. *Phys. Rev. Lett.* 80: 3779.

175 Sethi, R. and Barron, A.R. (2009). Characterization of single-walled carbon nanotubes by Raman spectroscopy, a report of RICE University, Report number 2.

176 Pfeiffer, R., Kuzmany, H., Kramberger, C. et al. (2003). Unusual high degree of unperturbed environment in the interior of single-wall carbon nanotubes. *Phys. Rev. Lett.* 90: 225501.

177 Pimenta, M.A., Marucci, S., Empedocles, S. et al. (1998). Raman modes of metallic carbon nanotubes. *Phys. Rev. B* 58: 6016.

178 Jiang, C., Kempa, K., Zhao, J. et al. (2002). Strong enhancement of the Breit–Wigner–Fano Raman line in carbon nanotube bundles caused by plasmon band formation. *Phys. Rev. B* 66: 161404.

179 Dresselhaus, M.S. and Dresselhaus, G. (1981). Intercalation compounds of graphite. *Adv. Phys.* 30: 139.

180 Rao, A.M. (1997). Evidence for charge transfer in doped carbon nanotube bundles from Raman scattering. *Science* 388: 257.

181 Jorio, A. (2003). Resonance Raman spectra of carbon nanotubes by cross-polarized light. *Phys. Rev. Lett.* 90: 107403.

182 Maultzsch, J., Reich, S., and Thomsen, C. (2002). Raman scattering in carbon nanotubes revisited. *Phys. Rev. B* 65: 233402.

183 Maultzsch, J., Reich, S., Schlecht, U., and Thomsen, C. (2003). High-energy phonon branches of an individual metallic carbon nanotube. *Phys. Rev. Lett.* 91: 087402.

184 Saito, S. and Zettl, A. (2008). *Carbon Nanotubes: Quantum Cylinders of Graphene*. Elsevier.

185 Jushi, R.A., Venkataraman, L., Dresselhaus, M.S., and Dresselhaus, G. (1993). Phonon modes in carbon nanotubules. *Chem. Phys. Lett.* 209: 77.